PERTURBATIVE/NON-PERTURBATIVE ASPECTS OF TOPOLOGICAL STRING THEORY AND CONDENSED MATTER PHYSICS

A Dissertation

by

ZHAOJIE XU

Submitted to the Graduate and Professional School of
Texas A&M University
in partial fulfillment of the requirements for the degree of

DOCTOR OF PHILOSOPHY

Co-Chairs of Committee,	Dimitri Nanopolous
	Katrin Becker
Committee Members,	Teruki Kamon
	Eric Rowell
Head of Department,	Grigory Rogachev

August 2022

Major Subject: Physics

ABSTRACT

Recently some novel relations between topological strings on some toric Calabi-Yau threefolds and Bloch electrons moving in two-dimensional lattices under uniform magnetic flux was found. It turns out that the modular double duality plays an important role. We compute the density of states of the condensed matter side and show that it matches with the imaginary part of the derivative of quantum A-period. We will analyze the bandwidths in great detail and show that it is related to the quantum B-period of the topological string side.

DEDICATION

To my mother, my father and my grandparents.

ACKNOWLEDGMENTS

I would like to thank Professor Dimitri Nanopolous and Professor Katrin Becker for advising me during my time at Texas A&M University.

I would also like to thank Professor Teruki Kamon, Professor Eric Rowell and Professor Valery Pokrovsky for their guidance and teaching.

I am grateful to Yasuyuki Hatsuda, Tuo Jia and Yuji Sugimoto for collaboration on some works. I would also like to thank Qianfan Chen, William Linch III, Yonghui Qi, Aritra Saha, Kaijia Sun, Xin Tong, Xin Wang and Lutian Zhao for some useful discussions.

CONTRIBUTORS AND FUNDING SOURCES

Contributors

This work was supported by a dissertation committee consisting of Professors Dimitri V. Nanopoulos, Katrin Becker, and Teruki Kamon of the Department of Physics and Astronomy and Professor Eric Rowell of the Department of Mathematics.

The numerical analysis in Chapter III were conducted in part by Professor Yasuyuki Hatsuda of the Department of Physics, Rikkyo University. The analyses in Chapter IV were conducted in part by Professor Yasuyuki Hatsuda and Yuji Sugimoto of Department of Physics, Pohang University of Science and Technology.

All other work conducted for the thesis (or) dissertation was completed by the student independently.

Funding Sources

Graduate study was supported by an assistantship from Department of Physics and Astronomy.

NOMENCLATURE

ABJM theory	Aharony-Bergman-Jafferis-Maldacena theory
BPS invariant	Bogomol'nyi-Prasad-Sommerfield invariant
CY manifold	Calabi-Yau manifold
DOS	Density of States
GHM conjecture	Grassi-Hatsuda-Marin$\tilde{o}$ conjecture
HMO mechanism	Hatsuda-Moriyama-Okuyama mechanism
NS limit	Nekrasov-Shatashivili limit
SCFT	Supercorformal Field Theory
the TS/ST correspondence	the Topological String/ Spectral Theory correspondence

TABLE OF CONTENTS

Page

LIST OF FIGURES

FIGURE Page

LIST OF TABLES

TABLE Page

1. INTRODUCTION

String theory as a promising candidate for theory of everything has found its application in various kinds of fields such as number theory, enumerative geometry, particle phenomenology and cosmology etc. However, our description of this framework remains quite limited. If we take the practical view that our understanding of the theory relies on how good we can calculate the physical amplitudes, then only for regime where perturbation theory [1] works do we have full control so far. For some special background where duality can help us probe the strong coupling regime, the result is often approximate. Therefore the study of non-perturbative string theory remains an ongoing endeavour.

Recently there is some progress made in the area of topological string theory introduced by Witten [1]. Although topological string theory is a simplified version of standard string theory, it captures many important quantities of the physical string theory. Inspired by the result of several works [2, 3, 4, 5] on ABJM matrix model, it was found in [6] that there exists a non-perturbative completion of the topological string partition function for a special class of Calabi-Yau manifolds. Moreover, it's conjectured that those non-perturbative completed partition functions can solve the eigenvalue problems of the corresponding quantum curve of those CY manifolds. This conjecture is later known as the topological string/ spectral theory correspondence. Though this conjecture has not been proved rigorously, it has passed numerous tests [7, 8, 9] and no counterexamples has been encountered. The quantization condition introduced in [6] is shown to be equivalent to a generalized version [10] of Nekrasov-Shatashivili quantization condition [11] in [12].

Interestingly, it was found in [13] that the topological string on local $\mathbb{P}^1 \times \mathbb{P}^1$ not only solves the eigenvalue problem of the mirror curve of local $\mathbb{P}^1 \times \mathbb{P}^1$, but also encodes the information of Harper-Hofstadter model on the square lattice [14]. This result is later generalized to the connection between quantum geometry of local $\mathcal{B}_3$ geometry [15] and triangular lattice [16]. The results aforementioned mainly involve the quantum version of the A-period. Regarding the quantum B-period,

[1] Recent works show that we may not even understand some versions of perturbative string theory well.

it was shown in [17] that its quantum mechanical counterpart is the so-called non-perturbative A function introduced by Zinn-Justin and Jentschura [18, 19]. In [20], the one-instanton and the two-instanton expansions of the square lattice was analyzed in detail. The quantum B-period near the conifold point of local $\mathbb{F}_0$ is shown to be equal to the non-perturbative A function of the square lattice. This result is later generalized in [21] to a connection between local $\mathcal{B}_3$ geometry and honeycomb lattice [22]. Similar results for the triangular lattice were also obtained by the author of this thesis and the collaborators.

This dissertation is organized in the following way. In Section 2, we will brief review the topological string theory and the recent development which leads to the topological string/ spectral theory correspondence. In Section 3, the Harper-Hofstadter model on various lattice systems will be introduced; detailed analysis of the spectrum would be performed in the semiclassical region. Section 4 studies the quantum geometry of local $\mathcal{B}_3$ geometry and its relation to Harper-Hofstadter model on triangular lattice and honeycomb lattice; the quantum geometry of local $\mathbb{F}_0$, which is a blowdown limit of local $\mathcal{B}_3$, is shown to be related to Harper-Hofstadter model on the square lattice. Conclusions and discussions on open problems would be included in Section 5.

2. BRIEF REVIEW OF TOPOLOGICAL STRING THEORY

Topological string theory is a simplified version of physical string theory which was originally formulated by twisting the $\mathcal{N} = (2, 2)$ sigma model. After the topological twisting, we get two models called A model and B model. Mirror symmetry states that these two formulations are equivalent. Practically speaking, the main task of topological string theory is about calculating the topological string free energy, which captures many important information of the internal manifold and the lower dimensional gauge/supergravity theories resulting from compactification of string/M/F theory. In this paper, we mainly focus on the refined topological strings on toric Calabi-Yau threefolds in the Nekrasov-Shatashivili (NS) limit [11].

2.1 A model

For the A model, it's more convenient to work in the target space perspective. The free energy is defined as the generating function of Gromov-Witten invariants $N_g^{\mathbf{d}}$, where $\mathbf{d}$ denotes the degree and g the genus. The free energy is defined as the formal sum

$$F(\mathbf{t}, g_s) = \sum_{g\geq 0} g_s^{2g-2} F_g(\mathbf{t}) \tag{2.1}$$

At genus 0,

$$F_0(\mathbf{t}) = \frac{1}{6} a_{ijk} t^i t^j t^k + P_2(t) + \sum_{\mathbf{d}} N_0^{\mathbf{d}} e^{-\mathbf{d}\cdot\mathbf{t}} \tag{2.2}$$

where a_{ijk} denotes the classical intersection and $P_2(t)$ is an ambiguous term. The genus 1 free energy is given by

$$F_1(\mathbf{t}) = b_i t^i + \sum_{\mathbf{d}} N_1^{\mathbf{d}} e^{-\mathbf{d}\cdot\mathbf{t}} \tag{2.3}$$

At higher genus,

$$F_g(\mathbf{t}) = C_g + \sum_{\mathbf{d}} N_g^{\mathbf{d}} e^{-\mathbf{d}\cdot\mathbf{t}}, \qquad g \geq 2 \tag{2.4}$$

where C_g is the constant map contribution to the free energy. The total free energy is then given by

$$F(\mathbf{t}, g_s) = F^p(\mathbf{t}, g_s) + \sum_{g\geq 0}\sum_{\mathbf{d}} N_g^{\mathbf{d}} e^{-\mathbf{d}\cdot\mathbf{t}} g_s^{2g-2}, \tag{2.5}$$

where $F^p(\mathbf{t}, g_s)$ is the polynomial part

$$F^p(\mathbf{t}, g_s) = \frac{1}{6g_s^2} a_{ijk} t^i t^j t^k + b_i t^i + \sum_{g\geq 0} C_g g_s^{2g-2}. \tag{2.6}$$

The BPS part of the free energy could be resummed in terms of Goparkumar-Vafa invariants [23]

$$F^{GV}(\mathbf{t}, g_s) = \sum_{g\geq 0}\sum_{\mathbf{d}}\sum_{w\geq 1} \frac{1}{w} n_g^{\mathbf{d}} \left(2\sin\frac{w g_s}{2}\right) e^{-w\mathbf{d}\cdot\mathbf{t}}, \tag{2.7}$$

where $n_g^{\mathbf{d}}$ be the Goparkumar-Vafa invariants which take values in $\mathbb{Q}$. Topological strings on toric Calabi-Yau threefolds can have a one-parameter deformation called refined topological string theory. This could be understood by turning on the Ω background in 4d/5d supersymmetric gauge theories resulting from string/M theory compactification on toric CY threefolds. In the large volume limit, the refined topological free energy consists of a perturbative part and an instanton part. The perturbative contributions has the form

$$F^p_{\text{ref}}(\mathbf{t}, \epsilon_1, \epsilon_2) = \frac{1}{\epsilon_1\epsilon_2}\left(\frac{1}{6} a_{ijk} t^i t^j t^k + 4\pi^2 b_i^{\text{NS}} t^i\right) + b_i t^i - \frac{(\epsilon_1+\epsilon_2)^2}{\epsilon_1\epsilon_2} b_i^{\text{NS}} t^i. \tag{2.8}$$

The constants b_i^{NS} can be obtained by the refined holomorphic anomaly equation [24, 25]. The instanton contributions are given by

$$F^{\text{inst}}_{\text{ref}}(\mathbf{t}, \epsilon_1, \epsilon_2) = \sum_{j_L, j_R\geq 0}\sum_{\mathbf{d}}\sum_{w\geq 1} (-1)^{2j_L+2j_R} N^{\mathbf{d}}_{j_L, j_R} \frac{\chi_{j_L}(q_L^w)\chi_{j_R}(q_R^w)}{w(q_1^{w/2} - q_1^{-w/2})(q_2^{w/2} - q_2^{-w/2})} e^{-w\mathbf{d}\cdot\mathbf{t}}, \tag{2.9}$$

where

$$q_{1,2} = e^{\epsilon_{1,2}}, \qquad q_{L,R} = e^{(\epsilon_1 \mp \epsilon_2)/2}, \tag{2.10}$$

and $\chi_j(q)$ are SU(2) characters, say

$$\chi_j(q) = \frac{q^{2j+1} - q^{-2j-1}}{q - q^{-1}}. \tag{2.11}$$

The instanton part of the refined free energy can be calculated quite efficiently using the refined topological vertex formalism [26] in the large radius limit. The ordinary topological string theory can be recovered in the limit

$$F_{\text{top}}(\mathbf{t}, g_s) = F_{\text{ref}}(\mathbf{t}, g_s, -g_s) \tag{2.12}$$

There's another interesting limit to take which is the NS limit:

$$F_{\text{NS}}(\mathbf{t}, \hbar) = \lim_{\epsilon_1 \to 0} \epsilon_1 F(\mathbf{t}, \epsilon_1, \hbar) \tag{2.13}$$

2.2 B model

A toric Calabi-Yau threefold is a toric variety given by the symplectic quotient,

$$M = (\mathbb{C}^{k+3}/\mathcal{SR})/G, \tag{2.14}$$

where $G = (\mathbb{C}^*)^k$ and $\mathcal{SR}$ is the Stanley-Reisner ideal of G. The quotient is specified by a matrix of charges Q_i^α, $i = 0, \cdots, k+2$, $\alpha = 1, \cdots, k$. The group G acts on the homogeneous coordinates x_i as

$$x_i \to \lambda_\alpha^{Q_i^\alpha} x_i, \qquad i = 0, \cdots, k+2 \tag{2.15}$$

where $\alpha = 1, \cdots, k$, $\lambda_\alpha \in \mathbb{C}^*$, and $Q_i^\alpha \in \mathbb{Z}$. The toric variety can be understood as the vacuum configuration of a 2d $U(1)^k$ (2,2) gauged linear sigma model (GLSM). The supersymmetric ground state is constrained by

$$\sum_{i=1}^{k+3} Q_i^\alpha |x_i|^2 = r^\alpha, \qquad \alpha = 1, \cdots, k, \tag{2.16}$$

where r^α is the K$\ddot{a}$hler class. In general, the K$\ddot{a}$hler class takes complex value with the imaginary part given by a theta angle: $t^\alpha = r^\alpha + i\theta^\alpha$. Mirror symmetry which relates A model and B model needs the existence of R symmetry. In order to avoid R symmetry anomaly, one has to put the condition

$$\sum_{i=1}^{k+3} Q_i^\alpha = 0, \qquad \alpha = 1, \cdots, k. \tag{2.17}$$

which is the Calabi-Yau condition for the toric case.

The mirror to the toric Calabi-Yau was constructed in [27]. Define the Batyrev coordinates

$$z_\alpha = \prod_{i=1}^{k+3} x_i^{Q_i^\alpha}, \qquad \alpha = 1, \cdots, k, \tag{2.18}$$

and

$$H = \sum_{i=1}^{k+3} x_i \tag{2.19}$$

Without loss of generality, we can set x_1 to 0 and the remaining x_i can be expressed by x and y. There is still a reparameterization symmetry left [28]:

$$\begin{pmatrix} x \\ y \end{pmatrix} \to G \begin{pmatrix} x \\ y \end{pmatrix}, \qquad G \in SL(2, \mathbb{Z}). \tag{2.20}$$

The mirror geometry is described by

$$P(X, Y, u, v) = uv - H(X, Y, z_\alpha) = 0, \qquad \alpha = 1, \cdots, k, \tag{2.21}$$

where $X := e^x, Y := e^y$ and X, Y, u, v $\in \mathbb{C}$. The algebraic spectral curve

$$H(X, Y, z_\alpha) = 0, \tag{2.22}$$

describes a Riemann surface embedded in $\mathbb{C}^* \times \mathbb{C}^*$, which is called the mirror curve to the toric Calabi-Yau in the literature.

In this thesis, we focus on a special class of toric Calabi-Yau manifold called toric del Pezzo Calabi-Yaus, which are total space of canonical bundle on a del Pezzo surface: $\mathcal{O}(K_S) \to S$. Given the charge matrix Q_i^α, we introduce

$$\nu^{(i)} = (1, \nu_1^{(i)}, \nu_2^{(i)}), \qquad i = 1, \cdots, k+3, \tag{2.23}$$

which are 3-dimensional real vectors. They satisfy

$$\sum_{i=1}^{k+3} Q_i^\alpha \nu^{(i)} = 0. \tag{2.24}$$

In terms of these vectors, the mirror curve can be expressed as

$$H(e^x, e^y) = \sum_{i=1}^{k+3} x_i \exp\left(\nu_1^{(i)} x + \nu_2^{(i)} y\right). \tag{2.25}$$

The holomorphic 3-form of the mirror CY is given by

$$\Omega = \frac{du \wedge dx \wedge dy}{\partial_v P} = \frac{du \wedge dx \wedge dy}{u} \tag{2.26}$$

For standard/unrefined topological string, the periods of the 3-form are

$$t_i = \oint_{A_i} \Omega, \qquad \mathcal{F}_i = \oint_{B_i} \Omega. \tag{2.27}$$

where A_i and B_i are holomorphic 3-cycles. Integrating out the non-compact directions, the 3-forms get reduced to 1-forms and the periods become

$$t_i = \oint_{\alpha_i} y dx, \qquad \mathcal{F}_i = \oint_{\beta_i} y dx, \tag{2.28}$$

where α_i and β_i are appropriate 1-cycles. Special geometry tells us that the B-periods can be

written as derivative of a function called prepotential:

$$\frac{\partial F_0(t)}{\partial t_i} = \mathcal{F}_i = \oint_{\beta_i} y dx. \tag{2.29}$$

In some sense, our understanding of the unrefined topological string theory relies on how well we can compute this prepotential.

In the context of refined B model, x and y gets promoted to Hermitian operators $\mathbf{x}$ and $\mathbf{y}$ satisfying the commutation relation

$$[\mathbf{x}, \mathbf{y}] = i\hbar. \tag{2.30}$$

For each toric del Pezzo Calabi-Yau, we can associate an operator $\mathsf{O}(\mathbf{x}, \mathbf{y})$ of the form

$$\mathsf{O}(\mathbf{x}, \mathbf{y}) = \sum_{m,n \in \mathbb{Z}} a_{m,n} e^{m\mathbf{x}+n\mathbf{y}}, \qquad a_{m,n} \geq 0 \tag{2.31}$$

in such a way that we have a well-defined eigenvalue problem

$$\mathsf{O}(\mathbf{x}, \mathbf{y})|\psi_n> = e^{E_n}|\psi_n>, \qquad n \in \mathbb{N} \tag{2.32}$$

We can solve this eigenvalue problem by the standard numerical method for quantum mechanics. Otherwise, as we will show in the next section, the topological string can also solve this problem in an efficient manner.

2.3 The TS/ST correspondence

The topological string/ spectral theory correspondence, also known as Grassi-Hatsuda-Marinö conjecture, states that the eigenvalues of a certain class of trace-class operators could be read off from the generalized topological string partition function of some Calabi-Yau 3-fold whose quantized mirror curve is identical to those operators. This conjecture has not been proved mathematically but passed all numerical tests to date. It's quite unexpected that the original indications pointing to this conjecture comes from the study of ABJM theory[29], which is the worldvolume

theory of M2 branes probing $\mathbb{C}^4/\mathbb{Z}_k$ and is dual to M theory on $AdS_4 \times S^7/\mathbb{Z}_k$. With the development of localization technique, the partition function of the ABJM theory gets simplified to a matrix integral

$$Z_{ABJM}(N,k) = \frac{1}{N!^2}\int \frac{d^N\mu d^N\nu}{(2\pi)^{2N}} \frac{\prod_{i<j}[2\sinh(\frac{\mu_i-\mu_j}{2})]^2[2\sinh(\frac{\nu_i-\nu_j}{2})]^2}{\prod_{i,j}[2\cosh(\frac{\mu_i-\nu_j}{2})]^2} \exp\left[\frac{ik}{4\pi}\sum_i(\mu_i^2-\nu_i^2)\right] \tag{2.33}$$

where k is the Chern-Simons level and N is the rank of the gauge group. By using the Cauchy's determinant identity, the partition function can be written as

$$Z_{ABJM}(N,k) = \frac{1}{N!}\sum_{\sigma\in S_N}(-1)^{\mathrm{sgn}(\sigma)}\int d^N x \prod_{j=1}^{N}\rho(x_j, x_{\sigma(j)}) \tag{2.34}$$

where

$$\rho(x_1,x_2) := \frac{1}{2\pi k}\frac{1}{(2\cosh\frac{x_1}{2})^{1/2}}\frac{1}{2\cosh\frac{x_1-x_2}{2k}}\frac{1}{(2\cosh\frac{x_2}{2})^{1/2}} \tag{2.35}$$

Notice that if we define the quantum density matrix

$$\hat{\rho}(\mathbf{p},\mathbf{q}) := \frac{1}{(2\cosh\frac{\mathbf{q}}{2})^{1/2}}\frac{1}{2\cosh\frac{\mathbf{p}}{2}}\frac{1}{(2\cosh\frac{\mathbf{q}}{2})^{1/2}} \tag{2.36}$$

with

$$[\mathbf{q},\mathbf{p}] = i\hbar, \qquad \hbar = 2\pi k \tag{2.37}$$

then

$$\rho(x_1,x_2) = < x_1|\hat{\rho}(\mathbf{p},\mathbf{q})|x_2 > \tag{2.38}$$

and in the limit $\hbar \to 0$, the classical density operator turns out to be the inverse of the mirror curve of local $\mathbb{P}^1 \times \mathbb{P}^1$:

$$\rho_{\text{cl}} = \frac{1}{e^x + e^{-x} + e^y + e^{-y}}, \tag{2.39}$$

$$\left(x = \frac{p+q}{2}, \quad y = \frac{q-p}{2}\right). \tag{2.40}$$

If we introduce the grand partition function

$$\Xi(\mu,k) := 1+\sum_{N=1}^{\infty} Z_{ABJM}(N,k)e^{N\mu} \tag{2.41}$$

and the grand potential

$$J(\mu,k) := \log(\Xi(\mu,k)), \tag{2.42}$$

then the grand partition function can be written as a spectral determinant of quantum density matrix whose inverse being the quantum mirror curve of local $\mathbb{P}^1\times\mathbb{P}^1$:

$$\Xi(\kappa,\hbar) = \det(1+\hat{\rho}) = \prod_{n=0}^{\infty}(1+\kappa e^{-E_n}). \tag{2.43}$$

Here μ is the chemical potential and $\kappa = e^{\mu}$ is the fugacity. According to [30], the grand potential can be calculated by topological string and refined topological string in Nekrasov-Shatashivili limit on local $\mathbb{P}^1\times\mathbb{P}^1$:

$$J(\mu,k) = J^{(\mathrm{WS})}(\mu,k) + J^{\mathrm{WKB}}(\mu,k) \tag{2.44}$$

where

$$J^{(\mathrm{WS})}(\mu,k) = F_{\mathrm{top}}(\frac{2\pi}{\hbar}(t+i\pi),\frac{4\pi^2}{\hbar^2}), \tag{2.45}$$

$$J^{(\mathrm{WKB})}(\mu,k) = \frac{t(\hbar)}{2\pi}\frac{\partial F_{\mathrm{NS}}(t(\hbar),\hbar)}{\partial t} + \frac{\hbar^2}{2\pi}\frac{\partial}{\partial\hbar}\left(\frac{F_{\mathrm{NS}}(t(\hbar),\hbar)}{\hbar}\right) + \frac{2\pi}{\hbar}bt(\hbar) + A(\hbar), \tag{2.46}$$

where $A(\hbar)$ is a function that is independent of μ and the topological string side parameters are identified with parameters of ABJM theory as follows [1]:

$$\frac{4\mu}{k} + i = t, \tag{2.47}$$

Notice that both perturbative part and non-perturbative part of $J(\mu,k)$ got poles for $\hbar\in 2\pi\mathbb{Q}$ but the sum of them is an entire function, this is known as the HMO pole cancellation mechanism [5].

[1] Generally there are two Kahler moduli for local $\mathbb{P}^1\times\mathbb{P}^1$,since they differ by a constant we only write one modulus.

Here we present the most general statement of Grassi-Hatsuda-Mariño conjecture. [6, 8]. For a mirror curve Σ of a toric Calabi-Yau 3-fold X with genus g_Σ, there are g_Σ canonical forms for the curve,

$$\mathcal{O}_i(x,y) + \kappa_i = 0, \qquad i = 1, \cdots, g_\Sigma. \tag{2.48}$$

The different canonical forms of the curves are related by reparametrizations and overall factors,

$$\mathcal{O}_i + \kappa_i = \mathcal{P}_{ij}(\mathcal{O}_j + \kappa_j), \qquad i = 1, \cdots, g_\Sigma, \tag{2.49}$$

where $\mathcal{P}_{ij}$ is of the form e^{mx+ny}. Equivalently, we can write

$$\mathcal{O}_i = \mathcal{O}_i^{(0)} + \sum_{i \neq j} \kappa_j \mathcal{P}_{ij} \tag{2.50}$$

We perform the Weyl quantization and both sides of (2.50) gets promoted to Hermitian operators.

$$\mathsf{O}_i = \mathsf{O}_i^{(0)} + \sum_{i \neq j} \kappa_j \mathsf{P}_{ij}. \tag{2.51}$$

The operator $\mathsf{O}_i^{(0)}$ can be interpreted as the unperturbed operator, while the fugacity κ_j encodes different perturbations of it. Just as in the genus-1 case, the inverse of O, ρ, is of interest to us. We have

$$\rho_i = \mathsf{O}_i^{-1}, \qquad i = 1, \cdots, g_\Sigma, \tag{2.52}$$

and

$$\rho_i^{(0)} = (\mathsf{O}_i^{(0)})^{-1}, \qquad i = 1, \cdots, g_\Sigma. \tag{2.53}$$

In order to construct the generalized Fredholm/spectral determinant, we introduce the operators

$$\mathsf{A}_{jl} = \rho_j^{(0)} \mathsf{P}_{jl}, \qquad j, l = 1, \cdots, g_\Sigma, \tag{2.54}$$

We define the spectral determinant as

$$\Xi_X(\boldsymbol{\kappa};\hbar) = \det(1 + \sum_{l=1}^{g_\Sigma} \kappa_l \mathsf{A}_{jl}). \tag{2.55}$$

Now (2.44) to (2.46) gets generalized to

$$J_X(\boldsymbol{\mu},\boldsymbol{\xi};\hbar) = J_X^{\text{WS}}(\boldsymbol{\mu},\boldsymbol{\xi};\hbar) + J_X^{\text{WKB}}(\boldsymbol{\mu},\boldsymbol{\xi};\hbar), \tag{2.56}$$

$$J_X^{\text{WS}}(\boldsymbol{\mu},\boldsymbol{\xi};\hbar) = F_{\text{top}}(\frac{2\pi}{\hbar}\boldsymbol{t}(\hbar) + i\pi\boldsymbol{B}, \frac{4\pi^2}{\hbar^2}), \tag{2.57}$$

$$J_X^{\text{WKB}}(\boldsymbol{\mu},\boldsymbol{\xi};\hbar) = \frac{t_i(\hbar)}{2\pi}\frac{\partial F_{\text{NS}}(\boldsymbol{t}(\hbar),\hbar)}{\partial t_i} + \frac{\hbar^2}{2\pi}\frac{\partial}{\partial\hbar}\left(\frac{F_{\text{NS}}(\boldsymbol{t}(\hbar),\hbar)}{\hbar}\right) + \frac{2\pi}{\hbar}b_i t_i(\hbar) + A(\boldsymbol{\xi},\hbar). \tag{2.58}$$

where ξ are the mass parameters and the $\boldsymbol{B}$-field is defined as a constant integral vector up to an even lattice that satisfies the following property: for all triples of degree $\boldsymbol{d}$, spin j_L and j_R such that the refined BPS invariants is non-vanishing, they must satisfy

$$(-1)^{2j_L+2j_R-1} = (-1)^{\boldsymbol{B}\cdot\boldsymbol{d}}. \tag{2.59}$$

The main statement of GHM conjecture is that the generalized spectral determinant is given by

$$\Xi_X(\boldsymbol{\kappa};\hbar) = \sum_{\boldsymbol{n}\in\mathbb{Z}^{g_\Sigma}} \exp\left(J_X(\boldsymbol{\mu} + 2\pi i\boldsymbol{n},\boldsymbol{\xi};\hbar)\right). \tag{2.60}$$

As a corollary, the eigenvalues of the quantum mirror curve can be read off from the solutions of

$$\Xi_X(\boldsymbol{\kappa};\hbar) = 0. \tag{2.61}$$

2.4 Exact Nekrasov-Shatashivili quantization conditions

In [11], Nekrasov and Shatashivili discovered interesting correspondence between supersymmetric gauge theories and quantum integrable systems. In the so called Nekrasov-Shatashivili limit ($\epsilon_1 \to 0, \epsilon_2 = \hbar$), the Nekrasov partition function captures important data of certain quantum inte-

grable systems. To be more precise, Nekrasov and Shtashivili conjectured that the supersymmetric vacua equation

$$\exp(\partial_{a_I}\mathcal{W}(\vec{a};\hbar)) = 1, \tag{2.62}$$

of the NS free energy

$$\mathcal{W}(\vec{a};\hbar) = \lim_{\epsilon_1\to 0}\epsilon_1 \log Z_{\text{Nek}}(\vec{a};\epsilon_1,\epsilon_2=\hbar) \tag{2.63}$$

gives the Bethe ansatz equations for the corresponding integrable system. Here $\vec{a}$ denotes the collection of all Coulomb branch parameters. Geometric engineering of 4d/5d supersymmetric gauge theories tells us that the NS free energy is just the topological string free energy in the NS limit on Calabi-Yau X,

$$\mathcal{W}(\vec{a};\hbar) = F_{\text{NS}}(\boldsymbol{t};\hbar) \tag{2.64}$$

Here compactification on X gives rise to the corresponding supersymmetric gauge theory and the Coulomb parameters get identified with mass parameters of X. The supersymmetric vacua equation is expected to become Bohr-Sommerfeld like quantization condition on the B-model side:

$$C_{ij}\frac{\partial F_{\text{NS}}(\boldsymbol{t};\hbar)}{\partial t_j} = 2\pi(n_i+\frac{1}{2}), \qquad i=1,\cdots,g_\Sigma. \tag{2.65}$$

Since the left hand side of (2.65) has poles at $\hbar = 2\pi p/q$ ($p,q\in\mathbb{Z}$ and $\gcd(p,q)=1$), this naive quantization condition breaks down if $\hbar/2\pi$ is rational. For arbitrary $\hbar$, the spectrum calculated from this method is only approximate compared to the numerical results. So following the spirit of pole cancellation mechanism, Wang Zhang and Huang proposed an exact quantization condition [10] by making a non-perturbative completion of the LHS of (2.65):

$$C_{ij}\left(\frac{\partial F_{\text{NS}}(\boldsymbol{t};\hbar)}{\partial t_j}+\frac{\partial F_{\text{NS}}(\tilde{\boldsymbol{t}};\tilde{\hbar})}{\partial \tilde{t}_j}\right) = 2\pi(n_i+\frac{1}{2}), \qquad i=1,\cdots,g_\Sigma, \tag{2.66}$$

where $\tilde{\boldsymbol{t}} = 2\pi\boldsymbol{t}/hbar$ and $\tilde{\hbar} = 4\pi^2/\hbar$. Though the Grassi-Hatsuda-Mariñ o conjecture and the exact Nekrasov-Shatashivili quantization scheme hasn't been proved in a complete rigorous manner, they

have passed numerous numerical tests to date and it was shown in [12] that these two approaches are equivalent mathematically. It's also remarked in [31] that the non-perturbative NS free energy is related to the NS limit of Lockhart-Vafa partition function [32].

3.1 The Harper-Hofstadter Problem

In this section, we introduce the Harper-Hofstadter model which concerns Bloch electrons moving in uniform magnetic fields. If we plot the spectrum of this model over a wide range of rational flux values, the spectrum would show a fractal structure called the Hofstadter's butterfly [14]. We will briefly review the Hofstadter model for square lattice, triangular lattice and honeycomb lattice respectively.

3.1.1 Square lattice

We first consider electrons moving in a two-dimensional square lattice. We work in the tight binding approximation and consider only isotropic case, the Hamiltonian we are interested in is given by

$$H = \sum_{m,n} \left(c^\dagger_{m+1,n} c_{m,n} e^{A^x_{m,n}} + c^\dagger_{m,n+1} c_{m,n} e^{A^y_{m,n}} + \text{h.c.} \right) \tag{3.1}$$

where $c^\dagger_{m,n}(c_{m,n})$ is the creation (annihilation) operator at site (m, n) satisfying the commutation relations

$$\{c_{m,n}, c^\dagger_{m',n'}\} = \delta_{mm'}\delta_{nn'}, \qquad \{c_{m,n}, c_{m',n'}\} = 0, \qquad \{c^\dagger_{m,n}, c^\dagger_{m',n'}\} = 0 \tag{3.2}$$

We fix the gauge using the Landau gauge such that $A^y_{m,n} = 0, A^x_{m,n} = m\phi$. Under the rational flux $\phi/(2\pi) = p/q$ with p and q being coprime integers, The eigenvalue equation becomes a difference equation

$$e^{ik_y}\psi_{m+1} + e^{-ik_y}\psi_{m-1} + 2\cos(k_x + m\phi)\psi_m = E\psi_m \tag{3.3}$$

where k_x and k_y are momentum in the Brillouin zone and ψ_n are Bloch functions with period q. Under rational flux, the Hamiltonian has a simple matrix form

$$H(k_x,k_y)=\begin{pmatrix} 2\cos(k_x) & e^{-ik_y} & 0 & \dots & 0 & e^{ik_y} \\ e^{ik_y} & 2\cos(k_x+2\pi\frac{p}{q}) & e^{-ik_y} & \dots & 0 & 0 \\ 0 & e^{ik_y} & \ddots & \ddots & & \vdots \\ \vdots & & \ddots & \ddots & \ddots & \vdots \\ 0 & 0 & & \ddots & \ddots & e^{-ik_y} \\ e^{-ik_y} & 0 & \dots & \dots & e^{ik_y} & 2\cos(k_x+2\pi\frac{(q-1)p}{q}) \end{pmatrix} \tag{3.4}$$

so that the spectrum could be solved by computing the secular equation $\det(EI-H)=0$, i.e.

$$F_{p/q}(E,k_x,k_y)=\det\begin{pmatrix} A_0 & -e^{-ik_y} & 0 & \dots & 0 & -e^{ik_y} \\ -e^{ik_y} & A_1 & -e^{-ik_y} & \dots & 0 & 0 \\ 0 & -e^{ik_y} & \ddots & \ddots & & \vdots \\ \vdots & & \ddots & \ddots & \ddots & \vdots \\ 0 & 0 & & \ddots & \ddots & -e^{-ik_y} \\ -e^{-ik_y} & 0 & \dots & \dots & -e^{ik_y} & A_{q-1} \end{pmatrix}=0 \tag{3.5}$$

where $A_n=-2\cos(k_x+2\pi\frac{np}{q})+E$. Alternatively, one can also write the secular equation in the following form:

$$e^{iqk_y}\mathrm{Tr}\left[\begin{pmatrix} T_0 & -e^{-2ik_y} \\ 1 & 0 \end{pmatrix}\begin{pmatrix} T_1 & -e^{-2ik_y} \\ 1 & 0 \end{pmatrix}\cdots\begin{pmatrix} T_{q-1} & -e^{-2ik_y} \\ 1 & 0 \end{pmatrix}\right]+1=0 \tag{3.6}$$

where $T_n=e^{-ik_y}(E-2\cos(k_x+m\phi))$. Solving (3.10) numerically gives us detailed information about the band structure for the given flux. In general, we got q bands for $\phi=2\pi p/q$ with p and q coprime integers. As shown on the left of 3.1, the energy dispersion for $\phi=2\pi 3/5$ splits into 5 bands. If we plot the range of energy as a function of flux, we get a fractal structure known as

the Hofstadter's butterfly. If the magnetic field is turned off, the density of states is given by the

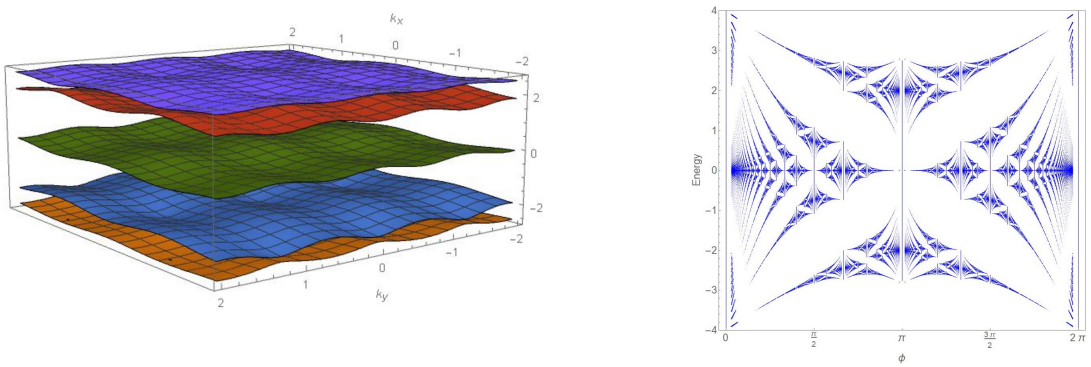

Figure 3.1: Left: the band structure for $\phi = 2\pi\frac{3}{5}$. Right: The Hofstadter's butterfly for the square lattice.

formula

$$\rho_0(E) = \iint_0^{2\pi} \frac{dk_x\, dk_y}{4\pi^2} \delta(2\cos k_x + 2\cos k_y - E). \tag{3.7}$$

Performing the integration, we get

$$\rho_0(E) = \frac{1}{2\pi^2}\mathbb{K}\left(1 - \frac{E^2}{16}\right). \tag{3.8}$$

The computation for rational flux is almost the same, the result is given in [33],

$$\rho(E) = \frac{P'(E)}{2\pi^2 b}\mathbb{K}\left(1 - \frac{P(E)^2}{16}\right), \tag{3.9}$$

where

$$P(E) = P_{p/q}(E) = F_{p/q}(E, 0, 0) + 4. \tag{3.10}$$

We plot the density of states for $\phi = 2\pi/3$ and $\phi = 6\pi/7$ in 3.2 as some examples. As we can see, at the middle of the subbands, the DOS hits some singularities. These singularities are called van Hove singularities that correspond to $P(E) = 0$.

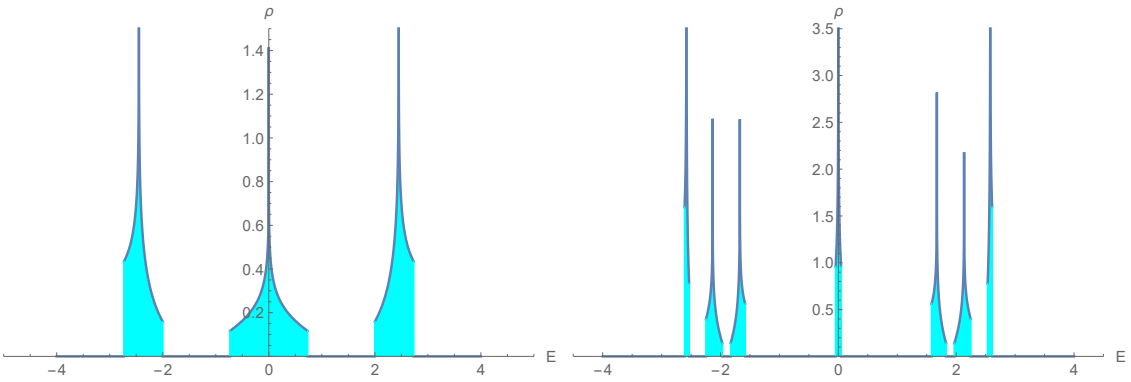

Figure 3.2: We show the density of states for the square lattice with isotropic parameters. The left figure is the graph for $\phi = 2\pi/3$), and the right is for $\phi = 6\pi/7$. The DOS is supported only on the energy subbands, and it has singularities at $P(E) = 0$.

3.1.2 Triangular lattice

We now turn to the Bloch electrons on the triangular lattice as shown in Fig. 3.3. Effectively, one can think of the Bloch electrons on triangular lattice as electrons moving in square lattice with the hopping parameter turned on for the $(1, 1)$ direction, see [34].

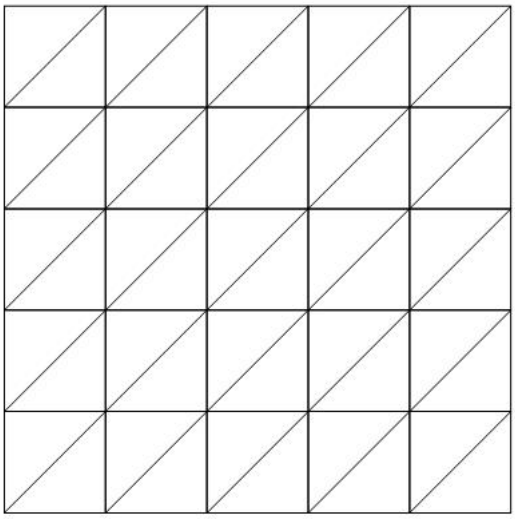

Figure 3.3: bipartite honeycomb lattice with lattice spacing a

The tight-binding Hamiltonian for the triangular lattice is given by

$$H = \sum_{m,n} \left(c^\dagger_{m+1,n} c_{m,n} e^{i\int_{(m,n)}^{(m+1,n)} \mathbf{A}\cdot\mathbf{dl}} + c^\dagger_{m,n+1} c_{m,n} e^{i\int_{(m,n)}^{(m,n+1)} \mathbf{A}\cdot\mathbf{dl}} + c^\dagger_{m+1,n+1} c_{m,n} e^{i\int_{(m,n)}^{(m+1,n+1)} \mathbf{A}\cdot\mathbf{dl}} + \text{h.c.} \right) \tag{3.11}$$

We can fix the gauge by taking $\mathbf{A} = (\mathbf{0}, \phi\mathbf{x}, \mathbf{0})$, then the difference equation for the triangular lattice is

$$e^{ik_x}(1 + e^{i(k_y+\phi n)})\psi_{n+1} + e^{-ik_x}(1 + e^{-i(k_y+\phi n)})\psi_{n-1} + 2\cos(k_x + n\phi)\psi_n = E\psi_n. \tag{3.12}$$

Again we can put the Hamiltonian in a matrix form for rational flux and the spectrum is determined by the characteristic polynomial

$$\begin{aligned} \mathcal{D}_{p/q}(E, k_x, k_y) &= \det(EI_{q\times q} - H_{\text{tri}}) \\ &= \det \begin{pmatrix} A_0 & B_0 & 0 & \dots & 0 & B^*_{q-1} e^{-iqk_y} \\ B^*_0 & A_1 & B_1 & \dots & 0 & 0 \\ 0 & B^*_1 & \ddots & \ddots & & \vdots \\ \vdots & & \ddots & \ddots & \ddots & \vdots \\ 0 & 0 & & \ddots & \ddots & B_{q-2} \\ B_{q-1} e^{iqk_y} & 0 & \dots & \dots & B^*_{q-2} & A_{q-1} \end{pmatrix} = 0 \end{aligned} \tag{3.13}$$

where $A_n = -2\cos(k_x + 2\pi\frac{np}{q}) + E$, $B_n = -e^{ik_x}(1 + e^{i(k_y+(2n+1)\frac{p}{q}\pi)})$[1] We solve the determinant 3.13 numerically and reproduce the band spectrum shown in [16]. Notice here for the triangular lattice the spectrum is not invariant under $\phi \to \phi + 2\pi$. Instead, it's invariant under $\phi \to 4\pi - \phi$.

[1] Here we have some slight sign differences with the characteristic polynomial in [15], this minor modification only affect the constant term.

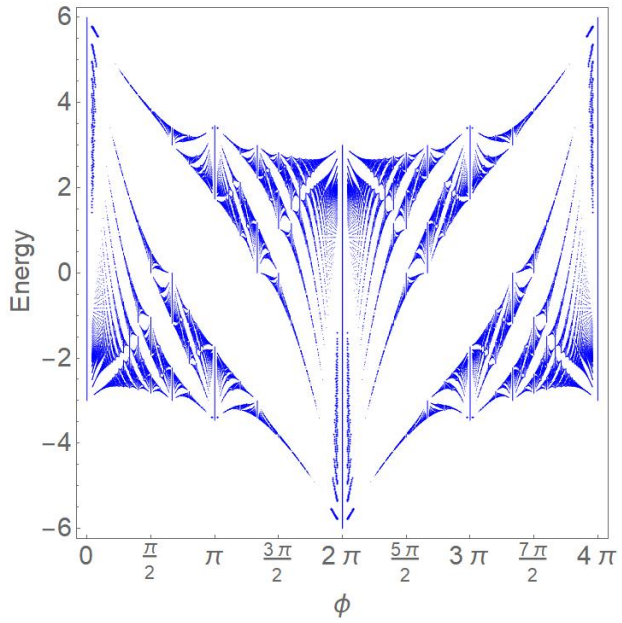

Figure 3.4: The Hofstadter's butterfly for the triangular lattice.

The DOS for the triangular lattice is given by

$$\rho(E) = \begin{cases} \dfrac{|F'|}{2\pi^2 b(3+F)^{1/4}} \mathbb{K}\left(\dfrac{12 - F^2 + 8\sqrt{3+F}}{16\sqrt{3+F}}\right), & -2 < F \leq 6, \\ \dfrac{2|F'|}{\pi^2 b\sqrt{12 - F^2 + 8\sqrt{3+F}}} \mathbb{K}\left(\dfrac{16\sqrt{3+F}}{12 - F^2 + 8\sqrt{3+F}}\right), & -3 \leq F < -2, \end{cases} \tag{3.14}$$

where $F = (-1)^{pq} F_{p/q}(E)$ and $F_{p/q}(E) = \mathcal{D}(E, 0, 0) + 2(3 + (-1)^p + (-1)^q + (-1)^{(p-1)q})$. It seems that for $b = 2$ this formula does not work, but in this case, we easily find

$$F_{a/2}(\mathcal{E}) = \mathcal{E}^2 - 6 \qquad (\text{odd } a). \tag{3.15}$$

The van Hove singularities for the triangular lattice correspond to the solutions of $F = -2$.

3.1.3 Honeycomb lattice

The honeycomb lattice is widely explored in the condensed matter literature. Materials like graphene are well known to have a single layer of honeycomb lattice structure. The Harper model

on the honeycomb lattice was discussed in [22]. The honeycomb lattice we are interested in is a

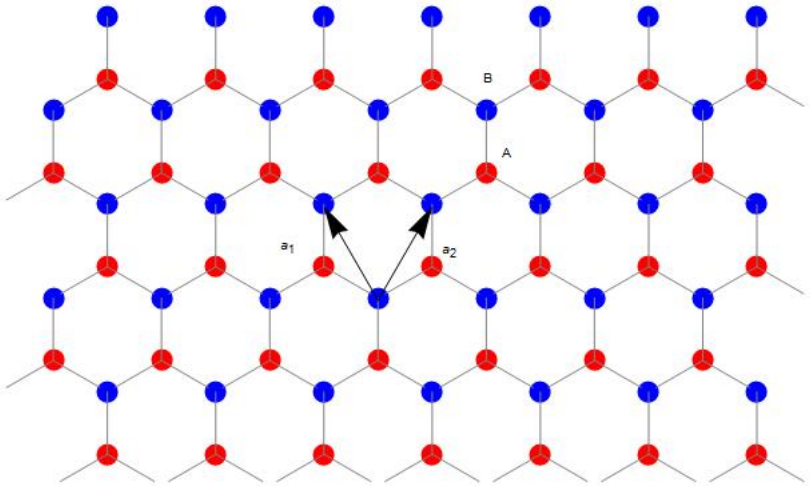

Figure 3.5: bipartite honeycomb lattice with lattice spacing a

bipartite system with two sublattices A and B as shown in Fig. 3.5. The primitive vectors are given by

$$\mathbf{a}_1 = (-\frac{\sqrt{3}}{2}a, \frac{3}{2}a), \qquad \mathbf{a}_2 = (\frac{\sqrt{3}}{2}a, \frac{3}{2}a), \tag{3.16}$$

where a is the lattice spacing constant. We can also work out the primitive vectors in the reciprocal space, which are give by

$$\mathbf{b}_1 = (-\frac{2\pi}{\sqrt{3}a}, \frac{2\pi}{3a}), \qquad \mathbf{b}_2 = (\frac{2\pi}{\sqrt{3}a}, \frac{2\pi}{3a}) \tag{3.17}$$

For simplicity, we first consider the case where the magnetic flux is turned off. In the tight binding approximation, we have the following eigenvalue equation

$$\begin{pmatrix} 0 & D(\mathbf{k}) \\ D^*(\mathbf{k}) & 0 \end{pmatrix} \begin{pmatrix} c_A \\ c_B \end{pmatrix} = E(\mathbf{k}) \begin{pmatrix} c_A \\ c_B \end{pmatrix}, \tag{3.18}$$

where $D(\mathbf{k}) := e^{-i\mathbf{d}_1\cdot\mathbf{k}} + e^{-i\mathbf{d}_2\cdot\mathbf{k}} + e^{-i\mathbf{d}_3\cdot\mathbf{k}}$ with

$$\mathbf{d}_1 = (-\frac{\sqrt{3}}{2}a, \frac{1}{2}a), \quad \mathbf{d}_2 = (\frac{\sqrt{3}}{2}a, \frac{1}{2}a), \quad \mathbf{d}_3 = (0, -a). \tag{3.19}$$

Therefore we can get the dispersion relation

$$E(\mathbf{k})^2 = D(\mathbf{k})^* D(\mathbf{k}) = 3 + 2\cos(\sqrt{3}k_x a) + 4\cos\left(\frac{3k_y a}{2}\right)\cos\left(\frac{\sqrt{3}k_x a}{2}\right) \tag{3.20}$$

From the dispersion relation, it's clear that the energy ranges from -3 to 3. For a generic point in the Brillouin zone, the system is normally gapped but near the corner of the first Brillouin zone, the gap closes up and forms the so-called Dirac cone, see Fig. 3.6. Near the Dirac cone, the electrons behave like massless relativistic fermions moving with the "speed of light" $3a/2$.

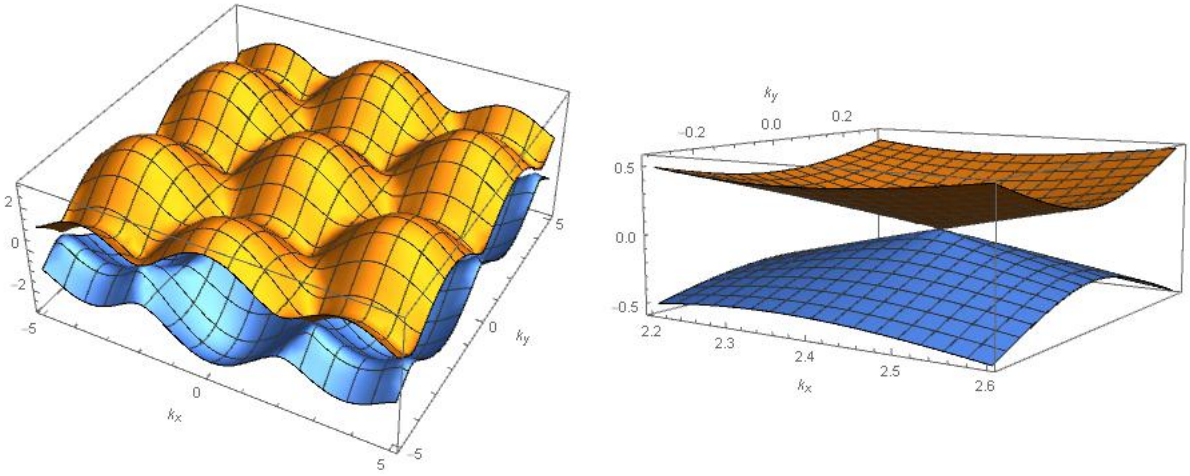

Figure 3.6: Left: the energy dispersion. Right: the Dirac cone near the corner of the Brillouin zone.

Now we turn on the magnetic flux, the function $D(\mathbf{k})$ gets replaced by a difference operator

$$D(\mathbf{k}) \to \hat{D} = e^{-\frac{i\phi}{12}} e^{\frac{i\phi y}{3a}} e^{-\frac{\sqrt{3}a}{2}\partial_x - \frac{a}{2}\partial_y} + e^{\frac{i\phi}{12}} e^{-\frac{i\phi y}{3a}} e^{\frac{\sqrt{3}a}{2}\partial_x - \frac{a}{2}\partial_y} + e^{a\partial_y} \tag{3.21}$$

under the Landau gauge $\mathbf{A} = (By, 0, 0)$. The phase factors $e^{\pm\frac{i\phi}{12}}$ come from the Baker-Campbell-Hausdorff formula and

$$\phi = 2\pi \frac{e\Phi}{hc}, \qquad \Phi = \frac{3\sqrt{3}a^2}{2} B. \tag{3.22}$$

The factor $3\sqrt{3}a^2/2$ simply comes from the area of the unit cell. The eigenvalue equation (3.18) thus gets promoted to two difference equations on two dimensions. Since we are using the Landau gauge, we can factorize the wavefunction as $\Psi_{A,B}(x, y) = e^{ik_x x}\psi_{A,B}(y)$. The difference equations further reduce to a set of difference equations of one dimension:

$$\begin{aligned} E\psi_A(y) &= 2\cos\left(\frac{\phi}{3a}y - \frac{\phi}{12} - \frac{\sqrt{3}a}{2}k_x\right)\psi_B\left(y - \frac{a}{2}\right) + \psi_B\left(y + a\right) \\ E\psi_B(y) &= 2\cos\left(\frac{\phi}{3a}y + \frac{\phi}{12} - \frac{\sqrt{3}a}{2}k_x\right)\psi_A\left(y - \frac{a}{2}\right) + \psi_A\left(y + a\right). \end{aligned} \tag{3.23}$$

By eliminating $\psi_A(y)$, one gets a single difference equation:

$$\begin{aligned} \lambda\psi_B(y) &= 2\cos\left(\frac{\phi}{3a}y + \frac{\phi}{12} - \frac{\sqrt{3}a}{2}k_x\right)\psi_B\left(y + \frac{3a}{2}\right) + 2\cos\left(\frac{\phi}{3a}y - \frac{5\phi}{12} - \frac{\sqrt{3}a}{2}k_x\right)\psi_B\left(y - \frac{3a}{2}\right) \\ &+ 2\cos\left(\frac{2\phi}{3a}y + \frac{\phi}{6} - \sqrt{3}ak_x\right)\psi_B(y), \end{aligned} \tag{3.24}$$

where $\lambda := E^2 - 3$. Let us write $\psi_n = \psi_B(\frac{3a}{2}n + \frac{a}{2})$. Then the above eigenvalue equation is finally reduced to the Harper's equation:

$$\lambda\psi_n = 2\cos\left(\frac{\phi}{2}n + \frac{\phi}{4} + \kappa\right)\psi_{n+1} + 2\cos\left(\frac{\phi}{2}n - \frac{\phi}{4} + \kappa\right)\psi_{n-1} + 2\cos\left(\phi n + \frac{\phi}{2} + 2\kappa\right)\psi_n, \tag{3.25}$$

where $\kappa = -\sqrt{3}ak_y/2$. If $\phi/(2\pi) = p/q$ is rational, then following the procedure of square lattice and triangular lattice, the spectrum of Bloch electrons on honeycomb lattice can be determined by

an equation of the similar form of Eq (3.13):

$$\mathcal{G}_{p/q}(\lambda,\kappa,\theta)=\det(H_{\text{honeycomb}}-\lambda I_{q\times q})=\det\begin{pmatrix} A_0 & B_0 & 0 & \dots & 0 & B^*_{q-1}e^{-i\theta k_y} \\ B^*_0 & A_1 & B_1 & \dots & 0 & 0 \\ 0 & B^*_1 & \ddots & \ddots & & \vdots \\ \vdots & & \ddots & \ddots & \ddots & \vdots \\ 0 & 0 & & \ddots & \ddots & B_{q-2} \\ B_{q-1}e^{i\theta k_y} & 0 & \dots & \dots & B^*_{q-2} & A_{q-1} \end{pmatrix}=0 \tag{3.26}$$

with $A_n=\cos\left(2\kappa-\frac{(2n+1)p}{q}\pi\right)-\lambda$ and $B_n=1+e^{i(2\kappa-\frac{(2n+1)p}{q}\pi)}$. Here θ is the Bloch angle due to the periodicity of Harper's equation. Similarly, once we got the spectral determinant, we

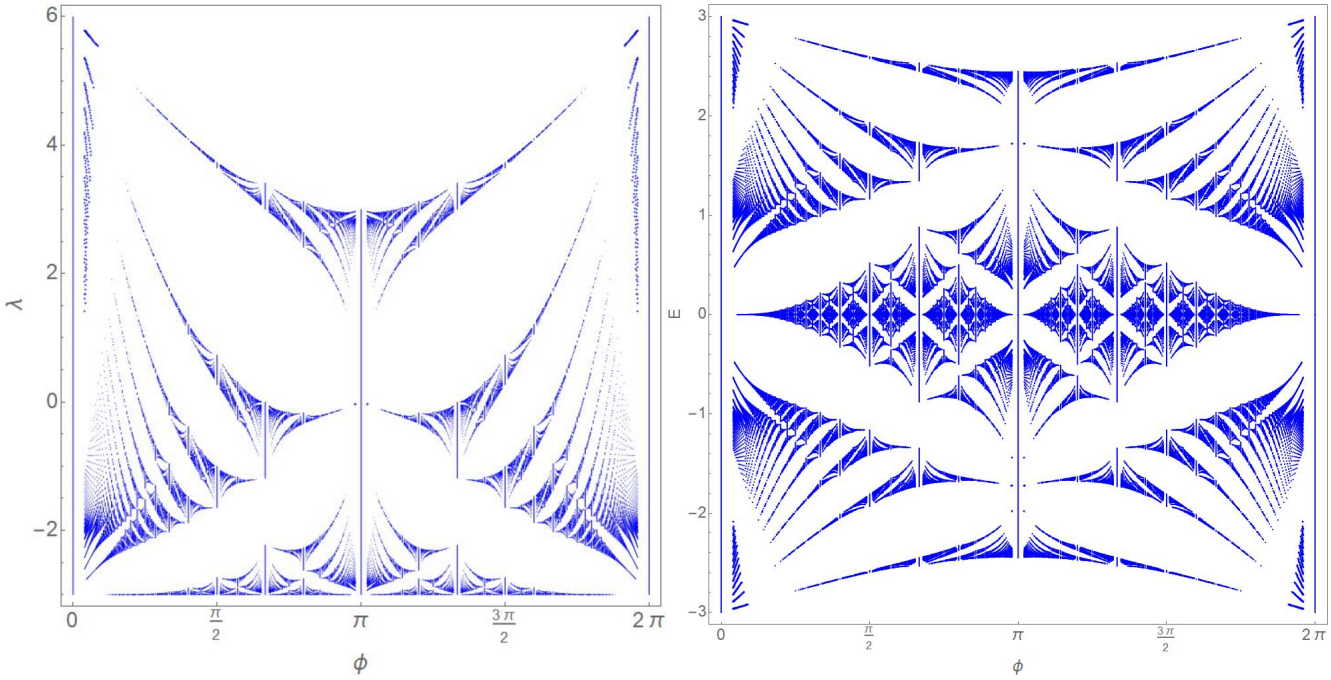

Figure 3.7: Left: the band spectrum for λ. Right: the band spectrum for E.

can plot the band spectrum for the honeycomb lattice, see Fig. 3.7. The form of the DOS for the honeycomb lattice is almost the same as the DOS for the triangular lattice because the Hamiltonian

for honeycomb lattice share the same form with the triangular lattice if the flux is turned off. For the redefined energy λ

$$\rho(\lambda) = \begin{cases} \dfrac{1}{2\pi^2 b(3+G)^{1/4}} \left|\dfrac{\partial G}{\partial \lambda}\right| \mathbb{K}\left(\dfrac{12-G^2+8\sqrt{3+G}}{16\sqrt{3+G}}\right), & -2 < G \leq 6, \\ \dfrac{2}{\pi^2 b\sqrt{12-G^2+8\sqrt{3+G}}} \left|\dfrac{\partial G}{\partial \lambda}\right| \mathbb{K}\left(\dfrac{16\sqrt{3+G}}{12-G^2+8\sqrt{3+G}}\right), & -3 \leq G < -2, \end{cases} \tag{3.27}$$

where

$$G = G_{a/b}(\lambda) = \mathcal{G}_{p/q}(\lambda, 0, 0) - \left(2(-1)^{pq} + 2(-1)^{q+1}(1+(-1)^{pq})\right). \tag{3.28}$$

The DOS for the real energy is simply

$$\rho(E) = \begin{cases} \dfrac{1}{2\pi^2 b(3+G)^{1/4}} \left|\dfrac{\partial G}{\partial E}\right| \mathbb{K}\left(\dfrac{12-G^2+8\sqrt{3+G}}{16\sqrt{3+G}}\right), & -2 < G \leq 6, \\ \dfrac{2}{\pi^2 b\sqrt{12-G^2+8\sqrt{3+G}}} \left|\dfrac{\partial G}{\partial E}\right| \mathbb{K}\left(\dfrac{16\sqrt{3+G}}{12-G^2+8\sqrt{3+G}}\right), & -3 \leq G < -2. \end{cases} \tag{3.29}$$

Here G is expressed as a polynomial of E, say $G(E^2-3)$.

3.2 Semi-classical Analysis

3.2.1 Perturbative series

The intricate structure of the band spectrum could be explained by the combination of the so-called T-symmetry and S-duality. For example, for the square lattice, the band spectrum is invariant under the shift $\phi \to \phi + 2\pi$. And under the inversion $\phi \to 2\pi^2/\phi$, the energy gets mapped to its "dual energy". These symmetry transformations make the band spectrum for our consideration fully non-perturbative, thus providing a perfect playground for studying perturbative/non-perturbative relations. In this section, we will first work out the weak flux expansion for all our models. Consider the Harper model for the square lattice, we can expand its Hamiltonian for small ϕ:

$$H_{\text{square}} = 4 - (\mathbf{p}_x^2 + \mathbf{p}_y^2)\phi + \frac{1}{12}(\mathbf{p}_x^4 + \mathbf{p}_y^4)\phi^2 - \frac{1}{360}(\mathbf{p}_x^6 + \mathbf{p}_y^6)\phi^3 + \cdots \tag{3.30}$$

We recognize the spectrum up to the first order as the Landau level of the electrons moving in the uniform magnetic field. Treat ϕ as the perturbation parameter, we can write [2]

$$E_n = \sum_{k=0}^{\infty} E_n^{(k)} \phi^k, \qquad |n\rangle = \sum_{k=0}^{\infty} \phi^k |n^{(k)}\rangle, \tag{3.31}$$

where $E_n^{(k)}$ is the n-th level energy shift at order k. Using a generalized version of the time-independent perturbation theory, we can work out the higher-order corrections order by order. The first few corrections are calculated as follows:

$$\begin{aligned} E_n^{(2)} &= \frac{1}{12}\langle n^{(0)}|(\mathbf{p}_x^4 + \mathbf{p}_y^4)|n^{(0)}\rangle, \\ E_n^{(3)} &= -\frac{1}{360}\langle n^{(0)}|(\mathbf{p}_x^6 + \mathbf{p}_y^6)|n^{(0)}\rangle + \sum_{m\neq n} \frac{|\langle m^{(0)}|(\mathbf{p}_x^4 + \mathbf{p}_y^4)|n^{(0)}\rangle|^2}{288(n-m)}. \end{aligned} \tag{3.32}$$

Alternatively, one can compute the perturbative expansion more efficiently by applying numerical techniques introduced by Bender and Wu [35, 36] (see also [37] for reference). Using these methods, we can calculate the perturbative expansion up to order $\sim \mathcal{O}(\phi^{100})$, here we show the first few orders:

$$\begin{aligned} E_{\text{top}}^{\text{square}} &= 4 - (2n+1)\phi + \frac{2n^2+2n+1}{8}\phi^2 - \frac{2n^3+3n^2+3n+1}{192}\phi^3 \\ &+ \frac{n^4+2n^3+6n^2+5n+2}{1536}\phi^4 + \frac{14n^5+35n^4+190n^3+250n^2+215n+67}{245760}\phi^5 + \mathcal{O}(\phi^6). \end{aligned} \tag{3.33}$$

Because the spectrum is symmetric under $E \to -E$, the expansion near the bottom edge is simply $E_{\text{btm}}^{\text{square}} = -E_{\text{top}}^{\text{square}}$. It's clear that the perturbative expansion (3.33) is not convergent for general level n. We can do a Borel resummation to cure the divergence. Because the Borel transform of (3.33) has poles on the positive axis of the Borel plane, we need to integrate along a line in the complex plane where no pole would be hitted [38]. The ambiguity of the Borel resummation is related to the imaginary part of instanton-anti-instanton fluctuation. Along the way, we can also work out the perturbative expansion of the wavefunction, here we show the unnormalized ground

[2] In the sense of weak flux expansion, the k-th order energy level in flux expansion corresponds to (k-1)-th order energy level in perturbation theory.

state wavefunction and the first-level wavefunction:

$$\psi_0(x;\phi) = e^{-\frac{x^2}{2}}\left[1 + \left(\frac{x^4}{48} - \frac{x^2}{16}\right)\phi + \left(\frac{x^8}{4608} - \frac{7x^6}{2304} + \frac{29x^4}{1536} - \frac{13x^2}{384}\right)\phi^2 + \mathcal{O}(\phi^3)\right] \tag{3.34}$$

$$\psi_1(x;\phi) = e^{-\frac{x^2}{2}}\left[2x + \frac{x^3(x^2-5)}{24}\phi + \frac{x^3(5x^6 - 90x^4 + 687x^2 - 1860)}{11520}\phi^2 + \mathcal{O}(\phi^3)\right] \tag{3.35}$$

The shortcoming of doing perturbation theory is that the perturbative wavefunction does not know the periodicity of the square lattice. Nevertheless, for weak flux, the perturbative expansion of energy matches with the exact ones pretty well. We plot the semiclassical expansion with the actual band spectrum. From the point of view of perturbative expansions, the bandwidths can be viewed as non-perturbative instanton corrections. For the triangular lattice, we can perform the

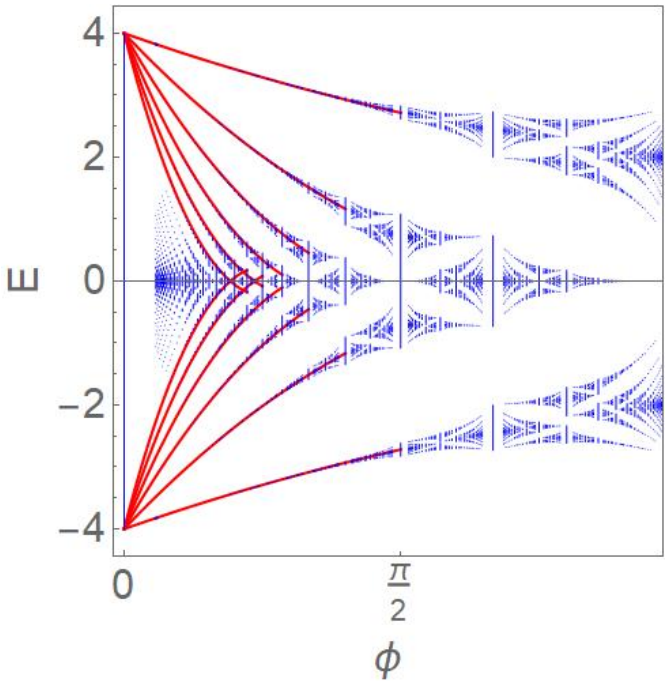

Figure 3.8: The perturbative expansion of (3.33) explains the Landau level splitting in the weak magnetic field limit. The red solid lines represent the perturbative expansion up to order $\mathcal{O}(\phi^5)$ for the first six energy levels.

same kind of numerical analysis for the weak flux expansion. The expansion around the top edge

is given by

$$E^{\text{tri}}_{\text{top}} = 6 - \sqrt{3}(1+2n)\phi + \frac{1+2n+2n^2}{4}\phi^2 - \frac{3+8n+6n^2+4n^3}{72\sqrt{3}}\phi^3 + \frac{3+8n+10n^2+4n^3+2n^4}{1728}\phi^4 - \frac{3+20n+45n^2+40n^3+15n^4+6n^5}{155520\sqrt{3}}\phi^5 + \mathcal{O}(\phi^6). \tag{3.36}$$

And near the bottom edge,

$$E^{\text{tri}}_{\text{btm}} = -3 + \sqrt{3}(n+\frac{1}{2})\phi - \frac{12n^2+12n+7}{24}\phi^2 + \frac{8n^3+12n^2+22n+9}{144\sqrt{3}}\phi^3 - \frac{336n^4+672n^3+1656n^2+1320n+433}{10368}\phi^4 + \frac{11424n^5+28560n^4+98960n^3+119880n^2+83650n+22797}{311040\sqrt{3}}\phi^5 + \mathcal{O}(\phi^6). \tag{3.37}$$

Thus we can plot the semiclassical expansion for the triangular lattice in Fig. 3.9. For the honeycomb lattice, the discussion is more involved. For the redefined energy λ, we have the following expansion near the top edge:

$$\lambda_{\text{top}} = 6 - \sqrt{3}(2n+1)\phi + \frac{3n^2+3n+1}{6}\phi^2 - \frac{n(n+1)(2n+1)}{36\sqrt{3}}\phi^3 + \frac{3n^4+6n^3+9n^2+6n+4}{2592}\phi^4 - \frac{6n^5+15n^4-80n^3-135n^2-190n-72}{155520\sqrt{3}}\phi^5 + \mathcal{O}(\phi^6). \tag{3.38}$$

And for the bottom edge,

$$\lambda_{\text{btm}}(n,\phi) = -3 + \sqrt{3}n\phi - \frac{n^2}{2}\phi^2 - \frac{n(n^2+2)}{18\sqrt{3}}\phi^3 - \frac{n^2(7n^2+20)}{216}\phi^4 - \frac{n(357n^4+2020n^2+470)}{9720\sqrt{3}}\phi^5 - \frac{n^2(961n^4+8950n^2+6670)}{58320}\phi^6 + \mathcal{O}(\phi^7). \tag{3.39}$$

We show the perturbative expansion together with the spectrum for λ on the left of Fig. 3.10. Notice for the lowest Landau level, λ_{btm} receives no perturbative corrections, say

$$\lambda_{\text{btm}}(0,\phi) = -3 \tag{3.40}$$

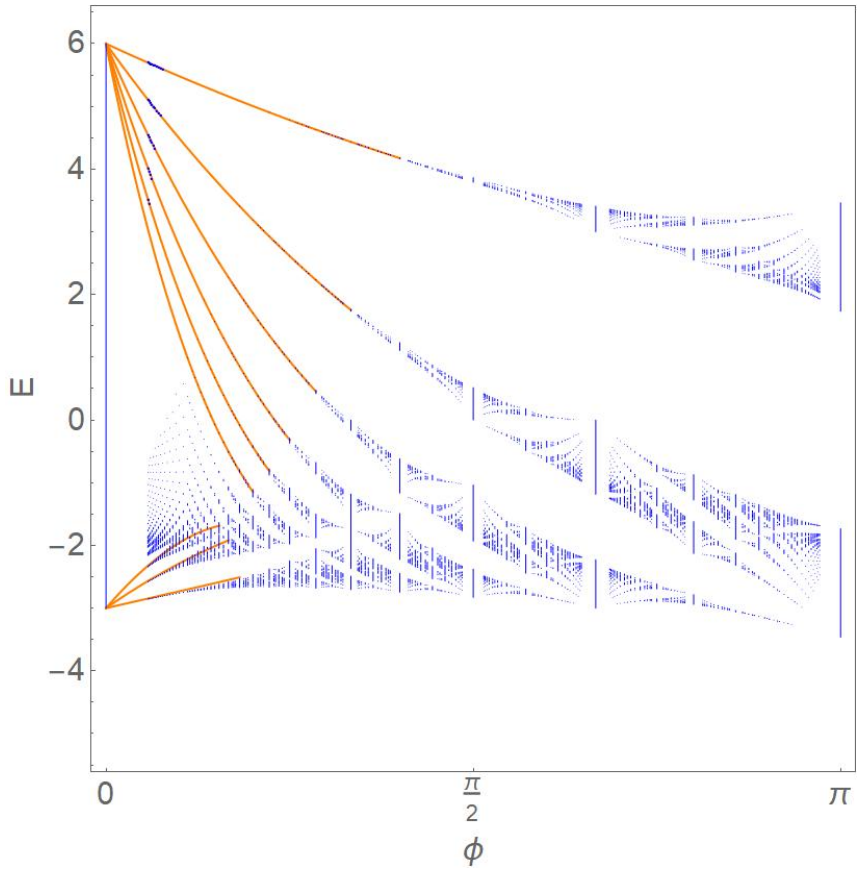

Figure 3.9: The perturbative expansion for the triangular lattice. The orange solid lines represent the perturbative expansion up to order $\mathcal{O}(\phi^4)$ for the first six energy levels for the top region and the first three energy levels for the bottom region.

The perturbative results for the honeycomb lattice was first found in [39] and in [39, 40, 41], it was argued that the honeycomb lattice model near the Dirac point has hidden supersymmetry, which could explain the behaviour of the lowest Landau level near the Dirac point. For the real energy E of the honeycomb lattice, the expansion of the top and the bottom edge is related to the expansion

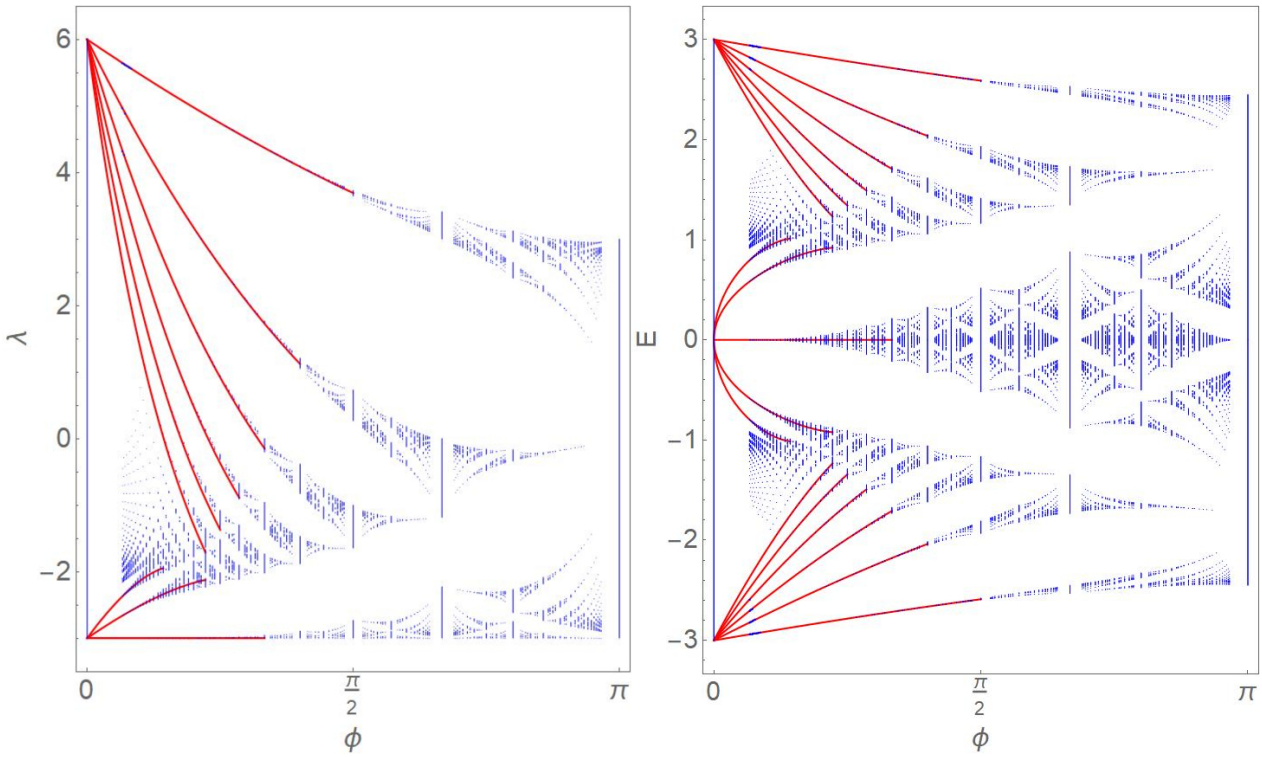

Figure 3.10: Left:The perturbative expansion for the redefined energy λ for the honeycomb lattice. The red solid lines represent the perturbative expansion up to order $\mathcal{O}(\phi^5)$ for the first six energy levels for the top region and the first three energy levels for the bottom region. Right: The perturbative expansion for the real energy E for the honeycomb lattice. We show the first six energy levels for the top and bottom region and the first three energy levels for the region near zero energy.

of λ_{top} by $E_{\text{top}} = \sqrt{\lambda_{\text{top}} + 3}$ and $E_{\text{btm}} = -\sqrt{\lambda_{\text{top}} + 3}$. To show it more explicitly,

$$\begin{aligned} E_{\text{top}}^{\text{honeycomb}} = -E_{\text{btm}}^{\text{honeycomb}} =& 3 - \frac{2n+1}{2}\sqrt{3}\phi + \frac{2n^2+2n+1}{72}\phi^2 + \frac{2n+1}{432\sqrt{3}}\phi^3 \\ &+ \frac{2n^4+4n^3+26n^2+24n+11}{31104}\phi^4 \\ &- \frac{14n^5+35n^4+320n^3+445n^2+380n+117}{933120\sqrt{3}}\phi^5 + \mathcal{O}(\phi^6). \end{aligned} \tag{3.41}$$

The expansion near the zero energy for E results from the expansion near the bottom edge for λ, we denote the expansion above the zero energy as E_+ and the expansion below the zero energy as

E_- such that $E_\pm = \pm\sqrt{\lambda_{\text{btm}} + 3}$, more explicitly,

$$\begin{aligned} E_{+}^{\text{honeycomb}} = - E_{-}^{\text{honeycomb}} = 3^{1/4}\sqrt{n}\sqrt{\phi} - \frac{n^{3/2}}{4\cdot 3^{1/4}}\phi^{3/2} - \frac{\sqrt{n}(17n^2+16)}{288\cdot 3^{3/4}}\phi^{5/2} \\ - \frac{n^{3/2}(73n^2+176)}{3456\cdot 3^{1/4}}\phi^{7/2} - \frac{\sqrt{n}(60281n^4+292960n^2+61440)}{2488320\cdot 3^{3/4}}\phi^{9/2} + \mathcal{O}(\phi^{11/2}). \end{aligned} \tag{3.42}$$

And for the lowest Landau level, $E_\pm$ is identically 0 due to the hidden supersymmetry.

3.2.2 Bandwidths analysis

As we mentioned in the last section, the bandwidths are invisible from perturbative analysis. In order to analyze the bandwidths, we need to include the non-perturbative corrections. We first review the non-perturbative results for the square lattice following [20]. The energy receives perturbative and instanton corrections in the following form

$$\begin{aligned} E_{(\theta_x,\theta_y)}(n,\phi) &= E^{\text{pert}}(n,\phi) + E^{\text{np}}_{(\theta_x,\theta_y)}(n,\phi) \\ &= \sum_{k=0}^{\infty} a_k^{(0)}(n)\phi^k + (2\cos\theta_x + 2\cos\theta_y)e^{-A/\phi}\mathcal{N}(n,\phi)\sum_{k=0}^{\infty} a_k^{(1)}(n)\phi^k + \mathcal{O}(e^{-2A/\phi}), \end{aligned} \tag{3.43}$$

where the Bloch angles are defined as $\theta_x = qk_x$ and $\theta_y = qk_y$ for $\phi = 2\pi p/q$. Here the band edges correspond to $(\theta_x, \theta_y) = (0,0)$ and (π,π). Since the van Hove singularity corresponds to $(\theta_x,\theta_y) = (\pi/2, \pi/2)$, therefore at the van Hove singularity the one-instanton correction vanishes.

We can determine the one-instanton fluctuation by doing numerical analysis of the bandwidths since the leading contribution to the bandwidths is given by the one-instanton expansion

$$\begin{aligned} \Delta E^{\text{square}}(n,\phi) :&= |E_{(0,0}(n,\phi) - E_{(\pi,\pi)}(n,\phi)| \\ &= 8|\mathcal{N}(n,\phi)|e^{-A/\phi}\sum_{k=0}^{\infty} a_k^{(1)}(n)\phi^k + \cdots, \end{aligned} \tag{3.44}$$

where the instanton action is calculated to be

$$A = \frac{1}{i}\int_0^{2\pi} \arccos(2-\cos x)\,dx = 8G. \tag{3.45}$$

Here G is Catalan's constant.

Using the spectral determinant (3.10) we can calculate the bandwidths numerically to high precision. By numerical fitting the first few Landau levels, we get

$$\Delta E^{\text{square}}(n,\phi) \approx \frac{8^{n+2}}{n!\pi^n}\left(\frac{\phi}{2\pi}\right)^{\frac{1}{2}-n} e^{-A/\phi}\mathcal{P}^{\text{inst}}_{\text{square}}, \tag{3.46}$$

where the one-instanton fluctuation is given by

$$\begin{aligned}\log \mathcal{P}^{\text{inst}}_{\text{square}} = &-\frac{6n^2+30n+19}{96}\phi - \frac{20n^3+102n^2+136n+27}{4608}\phi^2 \\ &- \frac{210n^4+1380n^3+2910n^3+2700n+893}{368640} + \mathcal{O}(\phi^4).\end{aligned} \tag{3.47}$$

We would like to focus on the instanton-anti-instanton (bion) sector of the two-instanton sector. The perturbative sector and the instanton-anti-instanton sector share the same topological charge. According to resurgence analysis [38, 42], the asymptotics of perturbative expansion encodes the information of all other non-perturbative series and the ambiguity of the perturbative expansion is related to the bion fluctuation. The large order behavior of $a_k^{(0)}(n)$ has the following form

$$a_k^{(0)}(n) = \frac{SC_n}{2\pi i(2A)^{k+2n}}\sum_{m=0}^{\infty}(k+2n-m-1)!a_m^{(1,1)}(n)(2A)^m + \cdots, \tag{3.48}$$

where S is the Stokes constant, which is related to the ambiguity of Borel resummation of perturbative series. C_n is an n-dependant constant and we normalize $a_0^{(1,1)}(n)$ to be 1. By utilizing the data of (3.33), we get $S = 128i$ and $C_n = \frac{2^{8n}}{(n!)^2}$ from numerical method. Since we have also fixed the instanton action (3.45), we can estimate $a_m^{(1,1)}(n)$ through numerical fitting. The bion fluctuation turns out to be

$$\begin{aligned}\log \mathcal{P}^{\text{bion}}_{\text{square}} = &-\frac{6n^2+18n+13}{48}\phi - \frac{20n^3+66n^2+100n+27}{2304}\phi^2 \\ &- \frac{210n^4+900n^3+2190n^3+1980n+653}{184320} + \mathcal{O}(\phi^4).\end{aligned} \tag{3.49}$$

The instanton fluctuation (3.47), the bion fluctuation (3.49) and the perturbative expansion (3.33)

are interrelated by the perturbative/non-perturbative threesome relation

$$\frac{\mathcal{P}^{\text{bion}}_{\text{square}}}{(\mathcal{P}^{\text{inst}}_{\text{square}})^2} = \left(\frac{1}{2\phi}\frac{\partial E^{\text{pert}}}{\partial n}\right)^{-1}, \tag{3.50}$$

which suggests us to introduce a new function $\mathcal{A}(n,\phi)$ by

$$\begin{aligned}\mathcal{P}^{\text{inst}}_{\text{square}} &= \frac{1}{2\phi}\frac{\partial E^{\text{pert}}}{\partial n}e^{-\mathcal{A}(n,\phi)},\\ \mathcal{P}^{\text{bion}}_{\text{square}} &= \frac{1}{2\phi}\frac{\partial E^{\text{pert}}}{\partial n}e^{-2\mathcal{A}(n,\phi)}.\end{aligned} \tag{3.51}$$

It turns out that this new function is the non-perturbative A function appearing in the Zinn-Justin-Jentschura exact quantization conditions [18, 19]. Since we have already calculated the perturbative series and the instanton fluctuation for the square lattice, the explicit form for the A function is thus given by

$$\begin{aligned}\mathcal{A}^{\text{square}}(n,\phi) = &\left(\frac{B^2}{16}+\frac{11}{192}\right)\phi + \left(\frac{5B^3}{1152}+\frac{49}{4608}\right)\phi^2\\ &+\left(\frac{7B^4}{12288}+\frac{77B^2}{24576}+\frac{889}{2949120}\right)\phi^3+\mathcal{O}(\phi^4),\end{aligned} \tag{3.52}$$

where $B = n+\frac{1}{2}$.

For triangular lattice the bandwidths is given by

$$\Delta E^{\text{tri}} = \begin{cases}\left|E(0,0)-E(\frac{4\pi}{3},\frac{2\pi}{3})\right| & \text{p odd},\\ \left|E(3\pi,\pi)-E(\frac{\pi}{3},-\frac{\pi}{3})\right| & \text{p even}.\end{cases} \tag{3.53}$$

Here $E(\theta_x,\theta_y)$ is the solution of (3.13). By numerical fitting we found the bandwidths near the top edge

$$\Delta E^{\text{tri}}_{\text{top}}(n,\phi) \approx \frac{108\cdot 3^{1/4}(6\sqrt{3})^n}{n!\pi^n}\left(\frac{\phi}{2\pi}\right)^{\frac{1}{2}-n} e^{-\hat{A}/\phi}\mathcal{P}^{\text{tri inst}}_{\text{top}}, \tag{3.54}$$

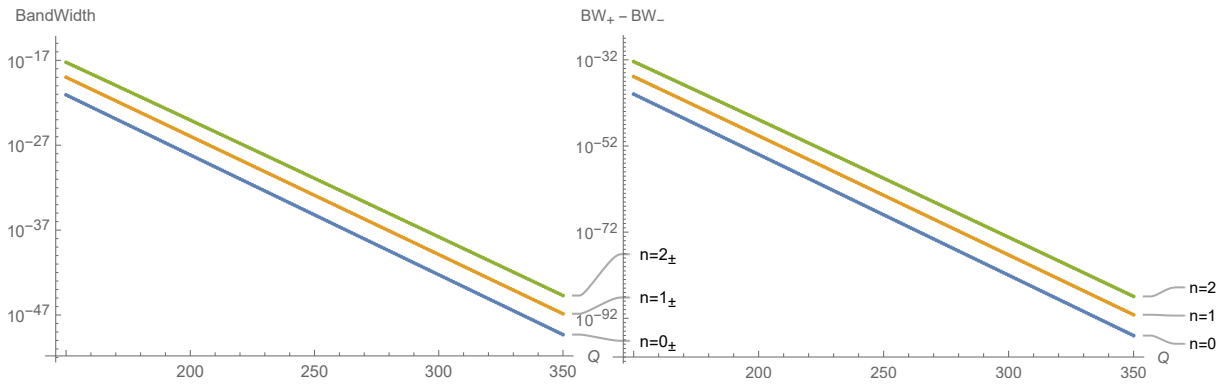

Figure 3.11: Left: the bandwidths near the bottom edge of the triangular lattice. Right: differences between those almost identical subbands.

and the bottom edge

$$\Delta E^{\text{tri}}_{\text{btm}\pm}(n,\phi) \approx \frac{9\cdot 3^{1/4}(3\sqrt{3})^n}{n!(2\pi)^n}\left(\frac{\phi}{2\pi}\right)^{\frac{1}{2}-n} e^{-\hat{A}/5\phi}\mathcal{P}^{\text{tri inst}}_{\text{btm}}, \tag{3.55}$$

where the instanton action is

$$\hat{A} = \frac{2}{i}\int_{-\pi/2}^{\pi/2} \arccos\left(\frac{2}{\cos x} - \cos x\right) dx = 10.149416064096\cdots. \tag{3.56}$$

The subscript $\pm$ denotes a pair of subbands whose bandwidths are almost identical. These overlapping subbands share the same one-instanton series but differ in two-instanton and higher-order instanton series. We show log plots of those pairs of bandwidths and their differences in 3.11. For convenience of our analysis, the flux is taken to be $\phi = 2\pi/Q$.

The instanton fluctuation near the top and bottom edge is given by

$$\begin{aligned}\log \mathcal{P}^{\text{tri inst}}_{\text{top}} = &-\frac{6n^2+42n+31}{72\sqrt{3}}\phi - \frac{2n^3+15n^2+23n-2}{864}\phi^2 \\ &- \frac{15n^4+138n^3+330n^2+153n-26}{46656\sqrt{3}}\phi^3 + \mathcal{O}(\phi^4),\end{aligned} \tag{3.57}$$

$$\begin{aligned}\log \mathcal{P}_{\text{btm}}^{\text{tri inst}} = &-\frac{30n^2+102n+59}{72\sqrt{3}}\phi - \frac{34n^3+147n^2+177n+72}{432}\phi^2 \\ &- \frac{4470n^4+26220n^3+48750n^2+46440n+15961}{58320\sqrt{3}}\phi^3 + \mathcal{O}(\phi^4).\end{aligned} \tag{3.58}$$

It's safe to assume that the bion fluctuation, instanton fluctuation and the perturbative series satisfy the threesome relation for both top and bottom edge:

$$\frac{\mathcal{P}^{\text{ bion}}}{(\mathcal{P}^{\text{ inst}})^2} = \left(\frac{1}{c\phi}\frac{\partial E^{\text{pert}}}{\partial n}\right)^{-1}, \tag{3.59}$$

where the normalization constant $c = -2\sqrt{3}$ for the top edge and $c = \sqrt{3}$ for the bottom edge. One can check this relation holds by doing resurgence analysis to get the coefficients of bion fluctuation. With this relation satisfied, we can proceed to calculate the non-perturbative A function near the top and bottom edge of the triangular lattice:

$$\begin{aligned}\mathcal{A}_{\text{top}}^{\text{tri}}(n,\phi) = &\left(\frac{23}{144\sqrt{3}} + \frac{B^2}{12\sqrt{3}}\right)\phi + \left(\frac{19B}{1728} + \frac{B^3}{432}\right)\phi^2 \\ &+ \left(-\frac{581}{746496\sqrt{3}} + \frac{97B^2}{31104\sqrt{3}} + \frac{5B^4}{15552\sqrt{3}}\right)\phi^3 + \mathcal{O}(\phi^4),\end{aligned} \tag{3.60}$$

$$\begin{aligned}\mathcal{A}_{\text{btm}}^{\text{tri}}(n,\phi) = &\left(\frac{31}{144\sqrt{3}} + \frac{5B^2}{12\sqrt{3}}\right)\phi + \left(\frac{37B}{288} + \frac{17B^3}{216}\right)\phi^2 \\ &+ \left(\frac{15443}{466560\sqrt{3}} + \frac{1075B^2}{3888\sqrt{3}} + \frac{149B^4}{1944\sqrt{3}}\right)\phi^3 + \mathcal{O}(\phi^4).\end{aligned} \tag{3.61}$$

The semiclassical analysis of the honeycomb lattice is very similar to the triangular lattice, but more subtler, as shown in [39, 21]. The bandwidths near the top edge of λ share the same form of (3.57). The only difference lies in the instanton fluctuation

$$\begin{aligned}\log \mathcal{P}_{\text{top}}^{\text{honeycomb inst}} = &-\frac{6n^2+42n+19}{72\sqrt{3}}\phi - \frac{2n^3+15n^2+15n+6}{864}\phi^2 \\ &- \frac{15n^4+138n^3+258n^2+297n+166}{46656\sqrt{3}}\phi^3 + \mathcal{O}(\phi^4),\end{aligned} \tag{3.62}$$

By numerical fitting, the bandwidths near the bottom edge has the following form

$$\begin{aligned}\Delta\lambda_{\text{btm}}(0,\phi) &\approx 9\sqrt{3}\left(\frac{2\pi}{\phi}\right)^{-1} e^{-\frac{2\hat{A}}{5\phi}}\mathcal{P}_{\text{btm}}^{\text{honeycomb bion}}(0,\phi),\\ \Delta\lambda_{\text{btm}}(n,\phi) &\approx \frac{3^{\frac{3(n+1)}{2}}\sqrt{n}}{\sqrt{2\pi}n!}\phi^{1-n}e^{-\frac{\hat{A}}{5\phi}}\mathcal{P}_{\text{btm}}^{\text{honeycomb inst}}(n,\phi), \qquad n\geq 1,\end{aligned} \tag{3.63}$$

where the instanton fluctuation is given by

$$\begin{aligned}\log\mathcal{P}_{\text{btm}}^{\text{honeycomb inst}} =& -\frac{30n^2+72n+11}{72\sqrt{3}}\phi - \frac{34n^3+96n^2+49n+16}{432}\phi^2\\ &- \frac{4470n^4+17280n^3+14910n^2+12960n+1081}{58320\sqrt{3}}\phi^3+\mathcal{O}(\phi^4).\end{aligned} \tag{3.64}$$

The leading contribution to the ground state bandwidths is related to the bion fluctuation instead of the instanton fluctuation due to the Dirac cone structure. By numerical fitting, the lowest level of the bion fluctuation is

$$\log\mathcal{P}_{\text{btm}}^{\text{honeycomb bion}}(0,\phi) = -\frac{11}{36\sqrt{3}}\phi - \frac{\phi^2}{27} - \frac{1081\phi^3}{29160\sqrt{3}}+\mathcal{O}(\phi^4). \tag{3.65}$$

For honeycomb lattice, we also have a pair of almost identical subbands near the bottom edge for $n\geq 1$. For convenience we have omitted the subscript $\pm$. The difference between those subbands turns out to be related to the two-instanton expansion $|\Delta\lambda_+(n,\phi)-\Delta\lambda_-(n,\phi)|\approx C_n e^{-\frac{2\hat{A}}{5\phi}}(1+\mathcal{O}(\phi))$.

The bion fluctuation near the top and bottom edge can be obtained from resurgent analysis of perturbative series (3.38) and (3.39). Near the top edge,

$$\begin{aligned}\log\mathcal{P}_{\text{top}}^{\text{honeycomb bion}}(n,\phi) =& -\frac{3n^2+12n+5}{18\sqrt{3}}\phi - \frac{4n^3+18n^2+18n+7}{864}\phi^2\\ &- \frac{30n^4+168n^3+354n^2+378n+251}{46656\sqrt{3}}\phi^3+\mathcal{O}(\phi^4).\end{aligned} \tag{3.66}$$

And near the bottom edge,

$$\begin{aligned}\log \mathcal{P}_{\text{btm}}^{\text{honeycomb bion}}(n,\phi) = &-\frac{30n^2+36n+11}{36\sqrt{3}}\phi - \frac{34n^3+48n^2+49n+8}{216}\phi^2 \\ &- \frac{4470n^4+8640n^3+14910n^2+6480n+1081}{29160\sqrt{3}}\phi^3 + \mathcal{O}(\phi^4).\end{aligned} \tag{3.67}$$

One can show that by taking $n = 0$, (3.67) indeed reduces to (3.65). The threesome relationship of instanton fluctuation, bion fluctuation and perturbative expansion of λ share the same form of the threesome relationship of triangular lattice (3.59). And indeed the bion fluctuations predicted by the threesome relationship matches with the resurgence calculation. The non-perturbative A function associated with λ near the top edge and bottom edge is thus given by

$$\begin{aligned}\mathcal{A}_{\text{top}}^{\text{honeycomb}}(n,\phi) = &\left(\frac{-1}{144\sqrt{3}} + \frac{B^2}{12\sqrt{3}}\right)\phi + \left(\frac{B}{576} + \frac{B^3}{432}\right)\phi^2 \\ &+ \left(\frac{1051}{746496\sqrt{3}} + \frac{49B^2}{31104\sqrt{3}} + \frac{5B^4}{15552\sqrt{3}}\right)\phi^3 + \mathcal{O}(\phi^4),\end{aligned} \tag{3.68}$$

$$\begin{aligned}\mathcal{A}_{\text{btm}}^{\text{honeycomb}}(n,\phi) = &\left(\frac{11}{72\sqrt{3}} + \frac{5n^2}{12\sqrt{3}}\right)\phi + \left(\frac{49n}{432} + \frac{17n^3}{216}\right)\phi^2 \\ &+ \left(\frac{1081}{58320\sqrt{3}} + \frac{497n^2}{1944\sqrt{3}} + \frac{149n^4}{1944\sqrt{3}}\right)\phi^3 + \mathcal{O}(\phi^4).\end{aligned} \tag{3.69}$$

In the next section we will show that the non-perturbative A function is related to the quantum free energy of topological strings on certain CY threefolds.

4. QUANTUM GEOMETRY OF LOCAL $\mathcal{B}_3$ AND TS/CM CORRESPONDENCE[1]

In this chapter, we will discuss the quantum geometry of local $\mathcal{B}_3$, which is a three-point blowup of local $\mathbb{P}_2$. We will illustrate the topological string/ condensed matter theory correspondence by showing several quantities like the derivative of the quantum A-period are related to the physical quantities of the condensed matter side.

4.1 Quantum Curve of local $\mathcal{B}_3$

It's known mathematically that the local $\mathbb{P}^2$ geometry, the canonical bundle over $\mathbb{P}^2$, can be blown up up to 8 points. They are denoted as local $\mathcal{B}_n$ $(n = 1 \cdots 8)$. Out of those eight geometries local $\mathcal{B}_3$ is of great interest to us because it's connected to the Harper-Hofstadter model on triangular lattice and honeycomb lattice. The local $\mathcal{B}_3$ geometry is a toric Calabi-Yau threefold that belongs to the toric del Pezzo Calabi-Yau manifolds. Since it's a toric del Pezzo Calabi-Yau manifold, we can simply encode its information to a toric diagram, see Fig. 4.1. From the point of view of string theory, The duality between Type IIA and Type IIB string theory gives us an alternative description of this geometry. To be more precise, M theory/Typer IIA on local $\mathcal{B}_3$ is dual to Typer IIB with (p,q) fivebrane webs whose configuration is identical to the dual web diagram of local $\mathcal{B}_3$ [43]. The resulting effective theory is 5d $\mathcal{N} = 1$ SU(2) superconformal field theory (SCFT) with $N_f = 2$ [44]. The SO(2) flavour symmetry and U(1) instanton symmetry gets enhanced to $\mathrm{E}_3 \simeq \mathrm{SU}(3) \times \mathrm{SU}(2)$ at a UV fixed point.

We can read off the toric data of local $\mathcal{B}_3$ from its toric diagram. And from the toric data, we get its classical curve:

$$e^x + e^y + e^{-x-y} + m_1 e^{-x} + m_2 e^{-y} + m_3 e^{x+y} = \mathcal{E} \tag{4.1}$$

Here (m_1, m_2, m_3) are mass parameters and $\mathcal{E}$ is the true modulus of the local $\mathcal{B}_3$ geometry, which

[1]Part of this chapter is reprinted with permission from "Calabi-Yau geometry and electrons on 2d lattices" by Y. Hatsuda, Y. Sugimoto and Z. Xu, 2017. Physical Review D 95.8 (2017): 086004. Copyright [2017] by APS.

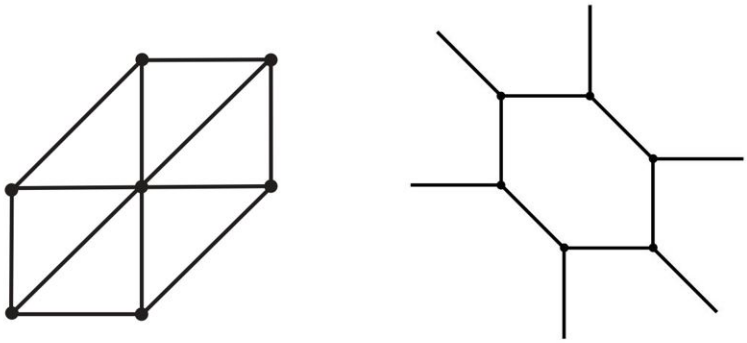

Figure 4.1: Left: the toric diagram of local $\mathcal{B}_3$. Right: the dual web diagram.

can be understood as energy. If we turn off the mass parameters $(m_1, m_2, m_3) \to (m_1, m_2, 0) \to (m_1, 0, 0) \to (0, 0, 0)$ in turn, the geometry is reduced to local $\mathcal{B}_2$, local $\mathbb{F}_1$ and local $\mathbb{P}^2$, respectively. Here $\mathbb{F}_n$ denotes the Hirzebruch surface $\mathcal{O} \oplus \mathcal{O}(-n)$. The blowdown of local $\mathcal{B}_3$ is not unique. With a different choice of the mass parameters, the mirror curve can be written as

$$e^x + e^y + m_1' e^{-x} + e^{-y} + m_2' e^{-x-y} + m_3' e^{x+y} = \mathcal{E} \tag{4.2}$$

If we turn off the mass parameters $(m_1', m_2', m_3') \to (m_1', m_2', 0) \to (m_1, 0, 0)$, we get local $\mathcal{B}_2$ and local $\mathbb{F}_0$ or local $\mathbb{P}_1 \times \mathbb{P}_1$, or in the geometry literature language $\mathcal{O}(-1, -1) \to \mathbb{P}_1 \times \mathbb{P}_1$, the canonical bundle over $\mathbb{P}_1 \times \mathbb{P}_1$. The physical equivalence of this blowdown process can be illustrated as follows. Consider the dual picture of (p,q) brane web of local $\mathcal{B}_3$, then removing one 7-brane from this (p,q) brane web corresponds to going from local $\mathcal{B}_3$ to local $\mathcal{B}_2$. By removing another 7-brane, we obtain the web corresponds to local $\mathbb{F}_0$.

The canonical way of quantizing the curve is to promote x and y to operators and impose the commutation relation:

$$[\mathsf{x}, \mathsf{y}] = i\hbar. \tag{4.3}$$

To avoid ambiguity of operator ordering, we take the following quantization method

$$e^{ax+by} \to e^{a\mathsf{x}+b\mathsf{y}} = q^{-ab/2} e^{a\mathsf{x}} e^{b\mathsf{y}}, \tag{4.4}$$

where $q = e^{i\hbar}$. Then the quantum curve of local $\mathcal{B}_3$ is simply given by

$$H = e^{\mathsf{x}} + e^{\mathsf{y}} + e^{-\mathsf{x}-\mathsf{y}} + m_1 e^{-\mathsf{x}} + m_2 e^{-\mathsf{y}} + m_3 e^{\mathsf{x}+\mathsf{y}}. \tag{4.5}$$

If we work in the x-representation, then $e^{\pm\mathsf{y}} = e^{\mp i\hbar\partial_x}$ are difference operators and the eigenvalue equation $H\psi(x) = \mathcal{E}\psi(x)$ leads to the difference equation

$$\begin{aligned} &e^x\psi(x) + \psi(x - i\hbar) + q^{-1/2}e^{-x}\psi(x + i\hbar) \\ &\quad + m_1 e^{-x}\psi(x) + m_2\psi(x + i\hbar) + m_3 q^{-1/2} e^x \psi(x - i\hbar) = \mathcal{E}\psi(x). \end{aligned} \tag{4.6}$$

Notice here there's similarity between the difference equation for the quantum mirror curve and the difference equation for the Harper model of the triangular lattice.

4.1.1 Classical Regime

The mirror curve (4.1) defines a genus-one Riemann surface. Under special geometry, we can define the A and B-period of the A and B-cycle of the Riemann surface:

$$t = \oint_A dx\, y(x, \mathcal{E}), \tag{4.7}$$

$$\frac{\partial F_0(t)}{\partial t} = \mathrm{vol}_0(\mathcal{E}) = \oint_B dx\, y(x, \mathcal{E}). \tag{4.8}$$

Here the B-period calculates the volume or area enclosed by the mirror curve in the phase space and $F_0(t)$ is the prepotential as introduced in Eq (2.29). At the technical level, there is an efficient way to compute these periods exactly. As explained in [45], the computation of these periods is

mapped to the periods for the Weierstrass normal form of the elliptic curve:

$$Y^2 = 4X^3 - g_2 X - g_3. \tag{4.9}$$

To go from the mirror curve (4.1) to the Weierstrass form (4.9), so-called Nagell's algorithm is used. See [45] in detail. We use the result (A.22) in [45] for computing the coefficients g_2 and g_3:

$$\begin{aligned}
g_2 &= \frac{1}{12z^4}[1 - 8(m_1+m_2+m_3)z^2 - 24(1+m_1m_2m_3)z^3 \\
&\quad + 16(m_1^2+m_2^2+m_3^2 - m_1m_2 - m_2m_3 - m_3m_1)z^4], \\
g_3 &= \frac{1}{216z^6}[1 - 12(m_1+m_2+m_3)z^2 - 36(1+m_1m_2m_3)z^3 \\
&\quad + 24(2m_1^2+2m_2^2+2m_3^2+m_1m_2+m_2m_3+m_3m_1)z^4 \\
&\quad + 144(m_1+m_2+m_3)(1+m_1m_2m_3)z^5 \\
&\quad + 8(-8m_1^3 - 8m_2^3 - 8m_3^3 + 12m_1^2m_2 + 12m_2^2m_3 + 12m_3^2m_1 \\
&\quad + 12m_1m_2^2 + 12m_2m_3^2 + 12m_3m_1^2 + 27 + 6m_1m_2m_3 + 27m_1^2m_2^2m_3^2)z^6],
\end{aligned} \tag{4.10}$$

where $z = 1/\mathcal{E}$. Then, the periods are written in closed forms

$$\begin{aligned}
\frac{\partial t}{\partial z} &= -\frac{1}{2\pi z^2}\frac{2}{\sqrt{e_1-e_3}}\mathbb{K}\left(\frac{e_2-e_3}{e_1-e_3}\right), \\
\frac{\partial^2 F_0}{\partial z \partial t} &= -\frac{1}{z^2}\frac{2}{\sqrt{e_1-e_3}}\mathbb{K}\left(\frac{e_1-e_2}{e_1-e_3}\right).
\end{aligned} \tag{4.11}$$

where $\mathbb{K}(m)$ is the complete elliptic integral of the first kind, and e_1, e_2 and e_3 are three roots of the elliptic curve (4.9). We have to choose them to reproduce the correct asymptotics of the A- and B-periods in $z \to 0$. The A-period has a logarithmic divergence, while the B-period has a double logarithmic divergence in this limit. The explicit forms of (e_1, e_2, e_3) are very complicated, but we

can fix them by the behavior in the limit $z \to 0$ as follows:

$$\begin{aligned} e_1 &= \frac{1}{6z^2} - \frac{2}{3}(m_1+m_2+m_3) - 2(1+m_1m_2m_3)z + \mathcal{O}(z^2), \\ e_2 &= -\frac{1}{12z^2} + \frac{1}{3}(m_1+m_2+m_3) + (1+m_1m_2m_3+2\sqrt{m_1m_2m_3})z + \mathcal{O}(z^2), \\ e_3 &= -\frac{1}{12z^2} + \frac{1}{3}(m_1+m_2+m_3) + (1+m_1m_2m_3-2\sqrt{m_1m_2m_3})z + \mathcal{O}(z^2). \end{aligned} \tag{4.12}$$

Plugging these expansions into the first equation in (4.11), one finds

$$\begin{aligned} -t = \log z &+ (m_1+m_2+m_3)z^2 + 2(1+m_1m_2m_3)z^3 \\ &+ \frac{3}{2}(m_1^2+m_2^2+m_3^2+4m_1m_2+4m_2m_3+4m_3m_1)z^4 + \mathcal{O}(z^5), \end{aligned} \tag{4.13}$$

where we fixed the integration constant so that $Q = e^{-t} = z + \mathcal{O}(z^2)$ in $z \to 0$. Inverting this, one gets the so-called mirror map

$$\begin{aligned} z = Q[1 &- (m_1+m_2+m_3)Q^2 - 2(1+m_1m_2m_3)Q^3 \\ &+ (m_1^2+m_2^2+m_3^2-m_1m_2-m_2m_3-m_3m_1)Q^4 + \mathcal{O}(Q^5)]. \end{aligned} \tag{4.14}$$

Similarly, from the second equation in (4.11), one obtains

$$\begin{aligned} \frac{\partial F_0}{\partial t} &= 3\log^2 z + \log(m_1m_2m_3)\log z + C_0 \\ &+ \left(\frac{1}{m_1}+\frac{1}{m_2}+\frac{1}{m_3}+m_1m_2+m_2m_3+m_3m_1\right)z \\ &+ \Bigg[(m_1+m_2+m_3)(\log(m_1m_2m_3)+6\log z) + 4(m_1+m_2+m_3) \\ &- \frac{1}{4m_1^2} - \frac{1}{4m_2^2} - \frac{1}{4m_3^2} - \frac{m_1^2m_2^2}{4} - \frac{m_2^2m_3^2}{4} - \frac{m_3^2m_1^2}{4}\Bigg]z^2 + \mathcal{O}(z^3). \end{aligned} \tag{4.15}$$

The integration constant C_0 is not fixed in this way. We fix it by comparing it to $\mathrm{vol}_0(\mathcal{E})$. From the numerical experiment, we observe the following asymptotic behavior of $\mathrm{vol}_0(\mathcal{E})$ in $\mathcal{E} \to \infty$:

$$\mathrm{vol}_0(\mathcal{E}) = 3\log^2\mathcal{E} - \log(m_1m_2m_3)\log\mathcal{E} - \pi^2 - \frac{1}{2}(\log^2 m_1 + \log^2 m_2 + \log^2 m_3) + \mathcal{O}(\mathcal{E}^{-1}). \tag{4.16}$$

Comparing this expansion with (4.15), the integration constant should be fixed by

$$C_0 = -\pi^2 - \frac{1}{2}(\log^2 m_1 + \log^2 m_2 + \log^2 m_3). \tag{4.17}$$

Substituting the mirror map (4.14) into (4.15), we finally obtain the prepotential

$$\begin{aligned} F_0(t) &= t^3 - \frac{\log(m_1 m_2 m_3)}{2} t^2 + C_0 t + \widetilde{C}_0 + F_0^{\text{inst}}(t), \\ F_0^{\text{inst}}(t) &= -\left(\frac{1}{m_1} + \frac{1}{m_2} + \frac{1}{m_3} + m_1 m_2 + m_2 m_3 + m_3 m_1\right) e^{-t} \\ &\quad - \frac{1}{8}\Bigg(16(m_1 + m_2 + m_3) - \frac{1}{m_1^2} - \frac{1}{m_2^2} - \frac{1}{m_3^2} \\ &\quad - m_1^2 m_2^2 - m_2^2 m_3^2 - m_3^2 m_1^2\Bigg) e^{-2t} + \mathcal{O}(e^{-3t}). \end{aligned} \tag{4.18}$$

Another integration constant $\widetilde{C}_0$ is not relevant in our analysis.

In particular, for $m_1 = m_2 = m_3 = 1$, things are much simpler. In this case, by shifting the y-variable by $y \to y - x/2$, the mirror curve becomes

$$2\cosh x + 4\cosh\frac{x}{2}\cosh y = \mathcal{E}. \tag{4.19}$$

Then the periods are written as

$$\begin{aligned} t(\mathcal{E}) &= \frac{1}{\pi i}\int_{x_-}^{x_+} dx\ \operatorname{arccosh}\left(\frac{\mathcal{E} - 2\cosh x}{4\cosh\frac{x}{2}}\right), \\ \frac{\partial F_0}{\partial t} &= 4\int_0^{x_-} dx\ \operatorname{arccosh}\left(\frac{\mathcal{E} - 2\cosh x}{4\cosh\frac{x}{2}}\right), \end{aligned} \tag{4.20}$$

where $x_\pm$ are defined for $\mathcal{E} > 6$ by

$$\frac{\mathcal{E} - 2\cosh x_\pm}{4\cosh\frac{x_\pm}{2}} = \mp 1, \qquad x_\pm > 0. \tag{4.21}$$

The integral in (4.20) can be analytically continued to $-3 \le \mathcal{E} \le 6$ with appropriate choice of cycle. We found that at the conifold point the classical A-period gives the instanton action (3.56)

of the triangular lattice and the constant part of the instanton action of the honeycomb lattice

$$\boxed{t(6) = \frac{5}{2}t(-3) = \frac{\hat{A}}{2\pi}.} \tag{4.22}$$

The fact that the period integral gives non-perturbative correction is explained in [3]. The derivative of these integrals with respect to $\mathcal{E}$ can be evaluated exactly. We find the following expressions:

$$\begin{aligned} \frac{\partial t}{\partial \mathcal{E}} &= \frac{2}{\pi\sqrt{\mathcal{E}^2 - 12 + 8\sqrt{\mathcal{E}+3}}}\mathbb{K}\left(\frac{16\sqrt{\mathcal{E}+3}}{\mathcal{E}^2 - 12 + 8\sqrt{\mathcal{E}+3}}\right), \\ \frac{\partial^2 F_0}{\partial \mathcal{E}\partial t} &= \frac{8}{\sqrt{\mathcal{E}^2 - 12 + 8\sqrt{\mathcal{E}+3}}}\mathbb{K}\left(\frac{\mathcal{E}^2 - 12 - 8\sqrt{\mathcal{E}+3}}{\mathcal{E}^2 - 12 + 8\sqrt{\mathcal{E}+3}}\right) \end{aligned} \tag{4.23}$$

From these, one immediately finds

$$-t = \log z + 3z^2 + 4z^3 + \frac{45}{2}z^4 + 72z^5 + 340z^6 + \mathcal{O}(z^7). \tag{4.24}$$

and

$$\begin{aligned} F_0(t) &= t^3 - \pi^2 t + \widetilde{C}_0 + F_0^{\text{inst}}(t), \\ F_0^{\text{inst}}(t) &= -6e^{-t} - \frac{21}{4}e^{-2t} - \frac{56}{9}e^{-3t} - \frac{405}{32}e^{-4t} - \frac{3756}{125}e^{-5t} - \frac{751}{9}e^{-6t} + \mathcal{O}(e^{-7t}). \end{aligned} \tag{4.25}$$

One can check that the functions

$$w_A(z) := \frac{\partial t}{\partial z}, \qquad w_B(z) := \frac{\partial^2 F_0}{\partial z \partial t}, \tag{4.26}$$

both satisfy the following second order differential equation

$$\begin{aligned} z^2(1+2z)(1+3z)(1-6z)w_i''(z) + z(3 - 4z - 120z^2 - 216z^3)w_i'(z) \\ +(1 - 2z - 96z^2 - 216z^3)w_i(z) = 0, \qquad i = A, B. \end{aligned} \tag{4.27}$$

This differential equation can be regarded as a Picard–Fuchs equation. Interestingly, we notice that

the same differential equation appears in the so-called mass deformed E_8 del Pezzo geometry with three non-vanishing masses studied in [7]. In appendix C of [15], it was shown that the mirror curve of E_8 del Pezzo geometry is simply a reparameterization of the mirror curve of local $\mathcal{B}_3$, which indicates that they should share the same quantum spectrum. In appendix B, we show that local $\mathcal{B}_3$ and mass deformed E_8 are indeed related by several steps of Hanany-Witten transitions for (p,q)-brane webs [43]. We would like to work out the periods for local $\mathbb{F}_0$ as well. Recall that with a different choice of mass parameters, the mirror curve of local $\mathcal{B}_3$ can be written as

$$e^x + e^y + m_1' e^{-x} + e^{-y} + m_2' e^{-x-y} + m_3' e^{x+y} = \mathcal{E}. \tag{4.28}$$

If we take the blowdown limit $m_2' \to 0$ and $m_3' \to 0$ and write $m = m_1'$, we get the mirror curve of local $\mathbb{F}_0$:

$$e^x + m e^{-x} + e^y + e^{-y} = \mathcal{E}. \tag{4.29}$$

We perform a change of variable $x \to x + \log m/2$ and define $\lambda := \sqrt{m}$, the periods of local $\mathbb{F}_0$ can be calculated analytically

$$\begin{aligned} t &= \frac{2}{\pi i} \int_{x_-}^{x_+} dx \ \operatorname{arccosh}\left(\frac{\mathcal{E}}{2} - \lambda \cosh x\right), \\ \frac{\partial F_0}{\partial t} &= 4 \int_0^{x_-} dx \ \operatorname{arccosh}\left(\frac{\mathcal{E}}{2} - \lambda \cosh x\right), \end{aligned} \tag{4.30}$$

where $x_\pm$ are defined for $\mathcal{E} > 2(1+\lambda)$ by

$$\frac{\mathcal{E}}{2} - \lambda \cosh x_\pm = \mp 1, \qquad x_\pm > 0. \tag{4.31}$$

The derivative of the classical period for local $\mathbb{F}_0$ was already calculated in various works, see [46, 7, 13]. Similar to the periods of local $\mathcal{B}_3$, the derivative of the periods of local $\mathbb{F}_0$ are written

in terms of the complete elliptic integral of the first kind:

$$\begin{aligned}\frac{\partial t}{\partial \mathcal{E}} &= \frac{4}{\pi\sqrt{\mathcal{E}^2-4(1-\lambda)^2}}\mathbb{K}\left(\frac{16\lambda}{\mathcal{E}^2-4(1-\lambda)^2}\right),\\ \frac{\partial^2 F_0}{\partial \mathcal{E}\partial t} &= \frac{8}{\sqrt{\mathcal{E}^2-4(1-\lambda)^2}}\mathbb{K}\left(\frac{\mathcal{E}^2-4(1+\lambda)^2}{\mathcal{E}^2-4(1-\lambda)^2}\right).\end{aligned} \tag{4.32}$$

One can do series expansion of the right-hand-side of the first equation of (4.32) and then integrate, the expansion for the classical A-period is given as follows:

$$\begin{aligned}-t =& \log z + 2(1+\lambda^2)z + 3(1+4\lambda^2+\lambda^4)z^2 + \frac{20}{3}(1+9\lambda^2+9\lambda^4+\lambda^6)z^3\\ &+ \frac{35}{2}(1+16\lambda^2+36\lambda^4+16\lambda^6+\lambda^8)z^4 + \mathcal{O}(z^5),\end{aligned} \tag{4.33}$$

where $z := 1/\mathcal{E}^2$. Inverting this, we get the mirror map for local $\mathbb{F}_0$:

$$\begin{aligned}z =& Q - (2+2\lambda^2)Q^2 + 3(\lambda^4+1)Q^3\\ &- 4(\lambda^6+\lambda^4+\lambda^2+1)Q^4 + 5(\lambda^8-5\lambda^4+1)Q^5 + \mathcal{O}(Q^6)\end{aligned} \tag{4.34}$$

Similarly, for the B-period, we get

$$\begin{aligned}\frac{\partial F_0}{\partial t} =& \log z^2 + 2\log z \log\lambda + C_0 + (4(1+\lambda^2)\\ &+ 4(1+\lambda^2)\log z + 4(1+\lambda^2)\log\lambda\, z + \mathcal{O}(z^2),\end{aligned} \tag{4.35}$$

where the integration constant is fixed to be $C_0 = -2\pi^2/3 - \log^2\lambda$. Substituting (4.34) into (4.35), we get the large radius expansion of the prepotential

$$\begin{aligned}F_0(t) &= \frac{1}{3}t^3 - \log\lambda\, t^2 + C_0 t + \tilde{C}_0 + F_{\text{inst}}(t),\\ F_{\text{inst}}(t) &= -4(\lambda^2+1)e^{-t} - \frac{1}{2}(\lambda^4+16\lambda^2+1)e^{-2t}\\ &\quad - \frac{4}{27}(\lambda^4+80\lambda^2+1)(\lambda^2+1)e^{-3t} + \mathcal{O}(e^{-4t}).\end{aligned} \tag{4.36}$$

One can check the above computation by solving the Picard-Fuchs equation of local $\mathbb{F}_0$ or using

the topological vertex technique [47] to calculate the large radius expansion.

For $\lambda = 1$, the classical periods can be written in closed form:

$$\begin{aligned} -t(z) &= \log z + 4z\,{}_4\mathrm{F}_3\left(1,1,\frac{3}{2},\frac{3}{2};2,2,2;16z\right), \\ \frac{\partial F_0}{\partial t} &= -2\pi^2 + \frac{2}{\pi}\mathrm{G}^{3,2}_{3,3}\left(\begin{matrix}0 & 0 & 0\\ \frac{1}{2} & \frac{1}{2} & 1\end{matrix}\middle| 16z\right), \end{aligned} \tag{4.37}$$

where ${}_p\mathrm{F}_q(a_1,\cdots,a_p;b_1,\cdots,b_q;z)$ is the hypergeometric function and

$$\mathrm{G}^{p,q}_{m,n}\left(\begin{matrix}a_1 & \cdots & a_p\\ b_1 & \cdots & b_q\end{matrix}\middle| z\right), \tag{4.38}$$

is the Meijer G function. At the conifold point (4.37) is proportional to the instanton action (3.45)

$$\boxed{t\left(z=\frac{1}{16}\right) = \frac{8G}{\pi} = \frac{A}{\pi}.} \tag{4.39}$$

4.1.2 The Quantum mirror map

The classical periods can be generalized to their quantum versions. For the B-period, its quantum version gives rise to the exact quantization condition and solves the spectral problem of the quantum curve. For the A-period, the quantum A-period was first proposed in [48] and several examples were calculated explicitly. In general, we can put the quantum mirror curve $(H(X,Y)-\mathcal{E})\psi(X)=0$ into the form

$$h(X,V(X);q,z,m_i) = 0, \tag{4.40}$$

where $X = e^x$, $Y = e^y$ and

$$V(X) = \frac{\psi(X)}{\psi(q^{-1}X)}. \tag{4.41}$$

Since $\log V(X)$ has finite number of poles in the small z expansion, we can get the small z expansion of the quantum A-period by calculating the residues:

$$-t = \log z + \oint \frac{dX}{2\pi i X} \log(V(X)) = \log z - \mathrm{Res}_{X=0} \frac{c}{X} \log(V(X)), \tag{4.42}$$

The constant c depends on which geometry we are considering. For local $\mathcal{B}_3$, we can calculate the quantum A-period order by order for arbitrary q. The difference equation written in the form (4.40) is given by

$$X + \frac{m_1}{X} + V(X) + \frac{m_2}{V(qX)} + \frac{q^{-1/2}}{XV(qX)} + m_3 q^{-1/2} X V(X) = \frac{1}{z}. \tag{4.43}$$

We expand $V(X)$ in z:

$$V(X) = \frac{v_{-1}(X)}{z} + v_0(X) + v_1(X) z + \cdots . \tag{4.44}$$

It is easy to fix each coefficient:

$$v_{-1}(X) = \frac{1}{1 + m_3 q^{-1/2} X}, \quad v_0(X) = -\frac{m_1 + q^{-1/2} X^2}{X(1 + m_3 q^{-1/2} X)}. \tag{4.45}$$

Then,

$$\log V(X) = \log \left(\frac{v_{-1}(X)}{z} \right) + \frac{v_0(X)}{v_{-1}(X)} z + \cdots . \tag{4.46}$$

The quantum A-period is obtained by the formula

$$\Pi_A(z; q) = -\mathrm{Res}_{X=0} \frac{V(X) - \log(v_{-1}(X)/z)}{X} = -\mathrm{Res}_{X=0} \left(\frac{v_0(X)}{X v_{-1}(X)} z + \cdots \right). \tag{4.47}$$

which turns out to be

$$\begin{aligned} -t = \log z + (m_1+m_2+m_3)z^2 + (q^{1/2}+q^{-1/2})(1+m_1m_2m_3)z^3 \\ + \left[\frac{3}{2}(m_1^2+m_2^2+m_3^2) + (4+q+q^{-1})(m_1m_2+m_2m_3+m_3m_1)\right]z^4 + \mathcal{O}(z^5), \end{aligned} \tag{4.48}$$

or inversely

$$\begin{aligned} \mathcal{E}^{-1} = z = Q - (m_1+m_2+m_3)Q^3 - (q^{1/2}+q^{-1/2})(1+m_1m_2m_3)Q^4 \\ + [m_1^2+m_2^2+m_3^2 - (q+q^{-1}-1)(m_1m_2+m_2m_3+m_3m_1)]Q^5 + \mathcal{O}(Q^6). \end{aligned} \tag{4.49}$$

In the classical limit $q \to 1$, it reduces to the classical A-period (4.13). Following the same procedure, we can also work out the quantum A-period of local $\mathbb{F}_0$, or the q-deformation of (4.33):

$$\begin{aligned} -t = \log z + 2(1+\lambda^2)z + 3\left(1+\frac{2}{3}(q+q^{-1}+4)\lambda^2+\lambda^4\right)z^2 \\ + \frac{2(\lambda^2+1)(3\lambda^2+3\lambda^2q^4+18\lambda^2q^3+2(5\lambda^4+19\lambda^2+5)q^2+18\lambda^2q)}{3q^2}z^3 + \mathcal{O}(z^4), \end{aligned} \tag{4.50}$$

The inverse series of (4.50) gives the quantum mirror map of local $\mathbb{F}_0$:

$$\begin{aligned} \mathcal{E}^{-2} = z = Q - 2(\lambda^2+1)Q^2 + (3\lambda^4 - (2\lambda^2(q^{1/2}-q^{-1/2})^2)+3)Q^3 \\ - \frac{2((\lambda^2+1)(2\lambda^4q^2+\lambda^2(q-1)^2(q^2+1)+2q^2))}{q^2}Q^4 + \mathcal{O}(Q^5) \end{aligned} \tag{4.51}$$

In the next section, we will show that the quantum A-period or its derivative can be written in closed form if q is a root of unity.

4.2 The TS/CM correspondence

It's shown in the TS/ST correspondence that the eigenvalue problem of the quantum mirror curve can be solved by the refined topological strings. We now know that for a special class of toric threefold like local $\mathcal{B}_3$ and local $\mathbb{F}_0$, the band spectrum of the Harper-Hofstadter model is identical to the branch cut structure of the Kähler modulus. Moreover, various quantities on both sides match with each other. This is the so-called topological string/condensed matter (TS/CM)

correspondence.

4.2.1 Branch cut structure of the Kähler modulus

The quantum A-period has some remarkable symmetry properties. First of all, it is invariant under the shift $\hbar \to \hbar + 4\pi$ and the flip $\hbar \to -\hbar$, namely

$$t(\mathcal{E}, m_i, \hbar + 4\pi) = t(\mathcal{E}, m_i, \hbar) = t(\mathcal{E}, m_i, -\hbar) = t(\mathcal{E}, m_i, 4\pi - \hbar). \tag{4.52}$$

This is the "T-symmetry". The exact quantization condition (2.66) is invariant under

$$(t, m_i, \hbar) \mapsto (\widetilde{t}, \widetilde{m}_i, \widetilde{\hbar}) = \left(\frac{2\pi t}{\hbar}, m_i^{2\pi/\hbar}, \frac{4\pi^2}{\hbar} \right). \tag{4.53}$$

This tells us that the energy and the "dual energy" is related implicitly by

$$t(\mathcal{E}, m_i; \hbar) = \frac{2\pi}{\hbar} t(\widetilde{\mathcal{E}}, \widetilde{m}_i; \widetilde{\hbar}). \tag{4.54}$$

The T and S-duality can be understood as a consequence of modular double symmetry of $\mathcal{U}_q(sl(2,\mathbb{R}))$[49]. Thanks to the modular double symmetry, we can work out the relation between $\mathcal{E}$ and $\widetilde{\mathcal{E}}$ by examining the difference equation and its dual. It can be proved without much effort that the Hamiltonian (4.5) commutes with its dual Hamiltonian:

$$\widetilde{H} = e^{\widetilde{\mathsf{x}}} + e^{\widetilde{\mathsf{y}}} + e^{-\widetilde{\mathsf{x}}-\widetilde{\mathsf{y}}} + \widetilde{m_1} e^{-\widetilde{\mathsf{x}}} + \widetilde{m_2} e^{-\widetilde{\mathsf{y}}} + \widetilde{m_3} e^{\widetilde{\mathsf{x}}+\widetilde{\mathsf{y}}}, \tag{4.55}$$

where

$$(\widetilde{\mathsf{x}}, \widetilde{\mathsf{y}}) = \left(\frac{2\pi}{\hbar}\mathsf{x}, \frac{2\pi}{\hbar}\mathsf{y} \right). \tag{4.56}$$

For simplicity we set $m_i = 1$ and shift the variable $y \to y - x/2$, we can write the difference equation and its dual as

$$\begin{aligned} 2\cosh\left(\frac{x}{2}+\frac{i\hbar}{4}\right)\Psi(x+i\hbar)+2\cosh\left(\frac{x}{2}-\frac{i\hbar}{4}\right)\Psi(x-i\hbar) &= (\mathcal{E}-2\cosh x)\Psi(x), \\ 2\cosh\left(\frac{\widetilde{x}}{2}+\frac{i\widetilde{\hbar}}{4}\right)\Psi(x+2\pi i)+2\cosh\left(\frac{\widetilde{x}}{2}-\frac{i\widetilde{\hbar}}{4}\right)\Psi(x-2\pi i) &= (\widetilde{\mathcal{E}}-2\cosh\widetilde{x})\Psi(x). \end{aligned} \tag{4.57}$$

These two equations share the same eigenfunction because of the compatibility of the two Hamiltonians. For $\hbar = 2\pi a/b$, the $b \times b$ secular equation should match with the $a \times a$ dual secular equation. The x-independent part of the secular equation is nothing but the secular equation for the triangular lattice, thus the algebraic relation between $\mathcal{E}$ and $\widetilde{\mathcal{E}}$ is given by

$$F_{a/b}(\mathcal{E}) = F_{b/a}(\widetilde{\mathcal{E}}). \tag{4.58}$$

Under the chain of T and S-transformations, we can write the quantum A-period in closed form. If ab is even, we can reduce the calculation to the classical period:

$$t(\mathcal{E}, \hbar = 2\pi a/b) = \frac{1}{b}\left(\log\widetilde{\mathcal{E}} - \Pi_A^{(0)}(\widetilde{\mathcal{E}})\right) \quad \text{for} \quad ab : \text{even}, \tag{4.59}$$

where

$$\widetilde{\mathcal{E}} = F_{a/b}(\mathcal{E}). \tag{4.60}$$

The derivative of the classical period is given by (4.23), therefore

$$\frac{\partial t(\mathcal{E}, \hbar = 2\pi a/b)}{\partial \mathcal{E}} = \frac{2}{\pi b}\frac{\partial \widetilde{\mathcal{E}}}{\partial \mathcal{E}}\frac{1}{\sqrt{\widetilde{\mathcal{E}}^2 - 12 + 8\sqrt{3+\widetilde{\mathcal{E}}}}}\mathbb{K}\left(\frac{16\sqrt{3+\widetilde{\mathcal{E}}}}{\widetilde{\mathcal{E}}^2 - 12 + 8\sqrt{3+\widetilde{\mathcal{E}}}}\right), \tag{4.61}$$

for ab even. The chain of reductions can be summarized by the following example

$$\frac{a}{b} = \frac{2}{7} \xrightarrow{\text{S}} \frac{7}{2} \xrightarrow{\text{T}} -\frac{1}{2} \xrightarrow{\text{T}} \frac{1}{2} \xrightarrow{\text{S}} 2 \xrightarrow{\text{T}} 0 \tag{4.62}$$

If ab is odd, the calculation of quantum A-period is reduced the the calculation of the quantum A-period at self-dual point $\hbar = 2\pi$:

$$t(\mathcal{E}, \hbar = 2\pi a/b) = \frac{1}{b}\left(\log \widetilde{\mathcal{E}} - \Pi_A^{(0)}(-\widetilde{\mathcal{E}})\right) \quad \text{for} \quad ab : \text{odd}, \tag{4.63}$$

The derivative of the quantum A-period at the self-dual point is given by

$$\frac{\partial t(\mathcal{E}, 2\pi)}{\partial \mathcal{E}} = \frac{2}{\pi\sqrt{\mathcal{E}^2 - 12 + 8\sqrt{3-\mathcal{E}}}}\mathbb{K}\left(\frac{16\sqrt{3-\mathcal{E}}}{\mathcal{E}^2 - 12 + 8\sqrt{3-\mathcal{E}}}\right), \tag{4.64}$$

then we have

$$\frac{\partial t(\mathcal{E}, \hbar = 2\pi a/b)}{\partial \mathcal{E}} = \frac{2}{\pi b}\frac{\partial \widetilde{\mathcal{E}}}{\partial \mathcal{E}}\frac{1}{\sqrt{\widetilde{\mathcal{E}}^2 - 12 + 8\sqrt{3-\widetilde{\mathcal{E}}}}}\mathbb{K}\left(\frac{16\sqrt{3-\widetilde{\mathcal{E}}}}{\widetilde{\mathcal{E}}^2 - 12 + 8\sqrt{3-\widetilde{\mathcal{E}}}}\right), \tag{4.65}$$

for ab odd. The basic flow of the reduction can be illustrated by the following example

$$\frac{a}{b} = \frac{3}{7} \overset{\text{S}}{\to} \frac{7}{3} \overset{\text{T}}{\to} \frac{1}{3} \overset{\text{S}}{\to} 3 \overset{\text{T}}{\to} 1 \tag{4.66}$$

Combining (4.61) and (4.65), we have

$$\frac{\partial t(\mathcal{E}, \hbar = 2\pi a/b)}{\partial \mathcal{E}} = \frac{2F'}{\pi b\sqrt{F^2 - 12 + 8\sqrt{3+F}}}\mathbb{K}\left(\frac{16\sqrt{3+F}}{F^2 - 12 + 8\sqrt{3+F}}\right), \tag{4.67}$$

where $F = (-1)^{ab}F_{a/b}$ as defined in section 3. The quantum A-period has branch cuts along $-3 \leq F \leq 6$. If we plot the intervals that correspond to the branch cuts as a function of $\hbar$, we get the exact same figure of the Hofstadter's butterf ly for the triangular lattice (Fig 3.4). Moreover, It was shown in [15] that the imaginary part of (4.67) equals the DOS of the triangular lattice (3.14):

$$\boxed{\rho(\mathcal{E}, \phi = 2\pi a/b) = \frac{1}{\pi}\left|\text{Im}\left(\frac{\partial t(\mathcal{E}, \hbar = 2\pi a/b)}{\partial \mathcal{E}}\right)\right|.} \tag{4.68}$$

This is one of the main results of this thesis. It turns out that if we choose a different quantization scheme for the mirror curve of local $\mathcal{B}_3$ other than (4.4), the spectral theory of it would correspond to the Harper-Hofstadter model on the honeycomb lattice. There are infinitely many ways of quantizing the operator e^{ax+by}. The second most natural way would be

$$e^{ax+by} = e^{ax}e^{by} \to e^{a\mathsf{x}}e^{b\mathsf{y}} = q^{ab/2}e^{a\mathsf{x}+b\mathsf{y}}, \tag{4.69}$$

Thus the Hamiltonian for $m_i = 1$ is of the form

$$H = e^{\mathsf{x}} + e^{\mathsf{y}} + e^{-\mathsf{x}} + e^{-\mathsf{y}} + q^{1/2}e^{\mathsf{x}+\mathsf{y}} + q^{-1/2}e^{-\mathsf{x}-\mathsf{y}}. \tag{4.70}$$

Notice that the same form of the quantum curve can also be obtained by setting $m_1' = 1, m_2' = q^{-1/2}$ and $m_3' = q^{1/2}$ in (4.28) and applying the first quantization method (4.4). This Hamiltonian is indistinguishable from the Hamiltonian for the honeycomb lattice after some change of variables, therefore it's better to denote the Kähler modulus as λ and the eigenvalue equation becomes $H\Psi(x) = \lambda\Psi(x)$. The small-z expansion of the quantum A-period gets modified to

$$\begin{aligned} -t(z;q) = \log z + 3z^2 + \frac{(1+q)^2}{q}z^3 + \left(3q + \frac{33}{2} + \frac{3}{q}\right)z^4 \\ + \frac{3(1+q)^2(1+4q+q^2)}{q^2}z^5 + \mathcal{O}(z^6). \end{aligned} \tag{4.71}$$

The S-dual relation for the quantum A-period would be

$$t(\lambda;\hbar) = \frac{2\pi}{\hbar}t(\widetilde{\lambda};\widetilde{\hbar}). \tag{4.72}$$

It's natural to conjecture the algebraic relation relating the Kähler modulus to its dual would be given by the spectral determinant of the honeycomb lattice. We would like to check whether it's

Table 4.1: The S-duality relation in local $\mathcal{B}_3$ for $m_i = 1$ for the quantization method (4.69). The energy λ at $\hbar = 2\pi a/b$ is related to the energy $\widetilde{\lambda}$ at $\widetilde{\hbar} = 2\pi b/a$ by the algebraic equation $G_{b/a}(\widetilde{\lambda}) = G_{a/b}(\lambda)$.

a	b	$G_{b/a}(\widetilde{\lambda}) = G_{a/b}(\lambda)$
1	1	$\widetilde{\lambda} = \lambda$
	2	$\widetilde{\lambda} = \lambda^2 - 6$
	3	$\widetilde{\lambda} = \lambda^3 - 9\lambda - 3$
	4	$\widetilde{\lambda} = \lambda^4 - 12\lambda^2 - 8\lambda + 6$
	5	$\widetilde{\lambda} = \lambda^5 - 15\lambda^3 - \frac{5}{2}(3+\sqrt{5})\lambda^2 + \frac{15}{2}(5-\sqrt{5})\lambda + 15$
	6	$\widetilde{\lambda} = \lambda^6 - 18\lambda^4 - 18\lambda^3 + 45\lambda^2 + 54\lambda + 3$
2	5	$\widetilde{\lambda}^2 - 6 = \lambda^5 - 15\lambda^3 - \frac{5}{2}(3-\sqrt{5})\lambda^2 + \frac{15}{2}(5+\sqrt{5})\lambda + 15$

true. Shifting $x \to x - y/2$ and $y \to x + y/2$, the difference equation and its S-dual would be

$$2\cosh\left(\frac{x}{2}+\frac{i\hbar}{4}\right)\Psi(x+i\hbar) + 2\cosh\left(\frac{x}{2}-\frac{i\hbar}{4}\right)\Psi(x-i\hbar) = \left(\lambda - 2\cosh\left(2x+\frac{i\hbar}{2}\right)\right)\Psi(x),$$
$$2\cosh\left(\frac{\widetilde{x}}{2}+\frac{i\widetilde{\hbar}}{4}\right)\Psi(x+2\pi i) + 2\cosh\left(\frac{\widetilde{x}}{2}-\frac{i\widetilde{\hbar}}{4}\right)\Psi(x-2\pi i) = \left(\widetilde{\lambda} - 2\cosh\left(2\widetilde{x}+\frac{i\hbar}{2}\right)\right)\Psi(x). \tag{4.73}$$

From these equations we find the algebraic relation relating λ and $\widetilde{\lambda}$ for $\hbar = 2\pi a/b$ is indeed given by

$$G_{a/b}(\lambda) = G_{b/a}(\widetilde{\lambda}), \tag{4.74}$$

where $G_{a/b}(\lambda)$ is defined in (3.28). We show some of these relations in the Table 4.1. And these relations satisfy (4.72). Notice that it suffices to show the relations for a/b between 0 and $1/2$ because for the second quantization method, the T-symmetry of the quantum A-period becomes

$$t(\lambda, \hbar) = t(\lambda, \hbar + 2\pi) = t(\lambda, -\hbar), \tag{4.75}$$

so a/b in the range between $1/2$ and 1 gets mapped to a number that belongs to the interval $[0, 1/2]$. Combining the T and S-transformations, we can write the quantum A-period in terms of

the classical A-period under the second quantization method (4.69)

$$t(\lambda;\hbar) = \frac{1}{b} t(\widetilde{\lambda};0). \tag{4.76}$$

The derivative of it can be written in closed form:

$$\frac{\partial t(\lambda,\hbar=2\pi a/b)}{\partial\lambda} = \frac{2}{\pi b\sqrt{G^2-12+8\sqrt{3+G}}}\frac{\partial G}{\partial\lambda}\,\mathbb{K}\left(\frac{16\sqrt{3+G}}{G^2-12+8\sqrt{3+G}}\right). \tag{4.77}$$

The quantum A-period as a function of λ has branch cuts along $-3 \le G(\lambda) \le 6$. If we plot the intervals as a function of $\hbar$, we get the branch cut structure for λ, which is identical to the left side of Fig 3.7. Similarly, if we plot the branch cuts along $-3 \le G(E^2-3) \le 6$ on the $E-\hbar$ plane, we obtain the Hofstadter's butterfly for the honeycomb lattice. Taking the imaginary part of (4.77), we find that it matches with the DOS of the redefined energy for the honeycomb lattice (3.27). If we take the derivative with respect to the real energy, then we get the DOS of the real energy (3.29). We summarize our results as follows:

$$\boxed{\begin{aligned}\rho(\lambda,\phi=2\pi a/b) &= \frac{1}{\pi}\left|\mathrm{Im}\left(\frac{\partial t(\lambda,\hbar=2\pi a/b)}{\partial\lambda}\right)\right|,\\ \rho(E,\phi=2\pi a/b) &= \frac{1}{\pi}\left|\mathrm{Im}\left(\frac{\partial t(\lambda=E^2-3,\hbar=2\pi a/b)}{\partial E}\right)\right|.\end{aligned}} \tag{4.78}$$

For the rest of this section, we would like to review the results in [13], in which the relations between quantum geometry of local $\mathbb{F}_0$ and Harper model on square lattice has been shown in great detail. The modular transformation property of the quantum A-period of local $\mathbb{F}_0$ is given by

$$\begin{aligned}\mathrm{T}: &\quad t(\mathcal{E},\lambda;\hbar) = t(\mathcal{E},\lambda;\hbar+2\pi) = t(\mathcal{E},\lambda;-\hbar),\\ \mathrm{S}: &\quad t(\mathcal{E},\lambda;\hbar) = \frac{2\pi}{\hbar}t(\widetilde{\mathcal{E}},\widetilde{\lambda};\widetilde{\hbar}).\end{aligned} \tag{4.79}$$

Because of the modular symmetry, the calculation of the quantum A-period can be reduced to the

calculation of the classical A-period if q is a root of unity:

$$t\left(\mathcal{E},\lambda;\hbar=\frac{2\pi a}{b}\right)=\frac{1}{b}t(\widetilde{\mathcal{E}},\lambda;0), \tag{4.80}$$

where $\mathcal{E}$ and $\widetilde{\mathcal{E}}$ is related by

$$P_{a/b}(\mathcal{E},\lambda)=P_{b/a}(\widetilde{\mathcal{E}},\widetilde{\lambda}). \tag{4.81}$$

Here $P_{a/b}(\mathcal{E},\lambda)$ is simply the anisotropic generalization of (3.10). In particular, if $\lambda=1$, then

$$t\left(\mathcal{E},1;\hbar=\frac{2\pi a}{b}\right)=-\frac{1}{b}\left(\log\widetilde{z}+4\widetilde{z}\,{}_4\mathrm{F}_3\left(1,1,\frac{3}{2},\frac{3}{2};2,2,2;16\widetilde{z}\right)\right),\qquad \widetilde{z}=\frac{1}{P_{a/b}(\mathcal{E})^2}. \tag{4.82}$$

The derivative of the quantum A-period can be written in closed form

$$\frac{\partial t(\mathcal{E},\lambda;\hbar=\frac{2\pi a}{b})}{\partial\mathcal{E}}=\frac{4P'}{\pi b\lambda^{\frac{b}{2}}\sqrt{P^2-4(1-\lambda)^2}}\mathbb{K}\left(\frac{16\lambda}{P^2-4(1-\lambda)^2}\right), \tag{4.83}$$

whose branch cut structure is identical to Hofstadter's butterfly for the square lattice (Fig. 3.1). Taking the imaginary part of (4.83), we get

$$\boxed{\rho(\mathcal{E})=\frac{1}{2\pi}\left|\mathrm{Im}\left(\frac{\partial t(\mathcal{E},\lambda,\hbar=2\pi a/b)}{\partial\lambda}\right)\right|.} \tag{4.84}$$

4.2.2 Free Energy near the conifold point

In this subsection we would like to investigate the quantum version of the B-period. The semi-classical region in the condensed matter physics side corresponds to those points near the conifold point in CY moduli space. So instead of working in the frame of large complex structure, we choose to work in the so-called conifold frame. For local $\mathcal{B}_3$, the periods near the conifold point $z=1/6$ can be defined as the solutions of the PF equation (4.27) with z substituted by $1/6-z_c$:

$$t_c(z_c)=z_c+\frac{9z_c^2}{2}+\frac{43z_c^3}{2}+\frac{429z_c^4}{4}+\frac{22077z_c^5}{40}+\mathcal{O}(z_c^6), \tag{4.85}$$

$$t_c^D(z_c) = \frac{\partial F_0}{\partial t_c} = t_c(z_c)\log z_c + \frac{z_c}{2} + \frac{25}{4}z_c^2 + \frac{305}{8}z_c^3 + \frac{10271}{48}z_c^4 + \mathcal{O}(z_c^5). \tag{4.86}$$

Inversing (4.85), we get the mirror map in the conifold frame

$$z_c = t_c - \frac{9t_c^2}{2} + 19t_c^3 - \frac{633t_c^4}{8} + \frac{13143t_c^5}{40} + \mathcal{O}(t_c^6). \tag{4.87}$$

Substituting (4.87) into (4.86) and integrate, we get the prepotential near the conifold point:

$$F_0(t_c) = \frac{t_c^2}{2}(\log\frac{-t_c}{2} - \frac{3}{2}) - \frac{t_c^3}{6} + \frac{t_c^4}{16} - \frac{t_c^5}{24} + \frac{59t_c^6}{1600} - \frac{11t_c^7}{280} + \mathcal{O}(t_c^8). \tag{4.88}$$

The quantum version of the prepotential is known as the quantum free energy

$$\mathcal{F}(t_c;\hbar) = \sum_{n\leq 0} F_{\text{NS}}^{(n)}(t_c)\hbar^{2n}. \tag{4.89}$$

Using holomor phic anomaly equations (see Appendix A), we can calculate F_{NS}^n recursively. The NS free energy at level one depends solely on the geometry of the curve and is given by (A.6). Expanding around the conifold point, we get

$$\begin{aligned} F_{\text{NS}}^{(1)}(t_c) = &-\frac{1}{24}\log t_c - \frac{23t_c}{24} + \frac{19t_c^2}{32} - \frac{97t_c^3}{144} \\ &+ \frac{1201t_c^4}{1280} - \frac{119t_c^5}{80} + \frac{23193t_c^6}{8960} - \frac{3077t_c^7}{640} + \mathcal{O}(t_c^8). \end{aligned} \tag{4.90}$$

Input this into the algorithm, we can get NS free energy to arbitrarily high orders up to some ambiguity needed to be fixed by the gap condition. We show the next few NS free energy

$$F_{\text{NS}}^{(2)}(t_c) = -\frac{7}{5760t_c^2} + \frac{581t_c}{1152} - \frac{18187t_c^2}{25600} - \frac{47t_c^3}{1920} + \frac{152191t_c^4}{30720} - \frac{124509t_c^5}{5120} + \frac{179973073t_c^6}{2048000} + \mathcal{O}(t_c^7), \tag{4.91}$$

$$\begin{aligned} F_{\text{NS}}^{(3)}(t_c) = &\frac{31}{161280t_c^4} + \frac{6553t_c}{3360} + \frac{41350369t_c^2}{3010560} - \frac{749749t_c^3}{10240} + \frac{3890269611t_c^4}{11468800} \\ &- \frac{18496964909t_c^5}{12902400} + \frac{355838787729t_c^6}{63078400} + \mathcal{O}(t_c^7). \end{aligned} \tag{4.92}$$

For the conifold point $z = -1/3$ which corresponds to the bottom edge, the A-period near this

point with coordinate $z_c = -1/3 - z$ is given by

$$t_c(z_c) = z_c + \frac{3z_c^2}{2} + 5z_c^3 + \frac{33z_c^4}{4} + \frac{189z_c^5}{5} + \frac{69z_c^6}{2} + \frac{2661z_c^7}{7} + \mathcal{O}(z_c^8). \tag{4.93}$$

Inverting this series, we get the mirror map

$$z_c = t_c - \frac{3t_c^2}{2} - \frac{t_c^3}{2} + \frac{99t_c^4}{8} - \frac{2157t_c^5}{40} + \frac{14397t_c^6}{80} - \frac{325923t_c^7}{560} + \mathcal{O}(t_c^8). \tag{4.94}$$

The lowest orders of the NS free energy is listed below:

$$F_0(t_c) = \frac{t_c^2}{2}(\log(-t_c^2)-3) - \frac{5t_c^3}{6} + \frac{17t_c^4}{16} - \frac{149t_c^5}{60} + \frac{12013t_c^6}{1600} - \frac{1481t_c^7}{56} + \frac{6475177t_c^8}{62720} + \mathcal{O}(t_c^9), \tag{4.95}$$

$$\begin{aligned} F_{\text{NS}}^{(1)}(t_c) = &-\frac{1}{12}\log t_c - \frac{31t_c}{24} + \frac{111t_c^2}{32} - \frac{1075t_c^3}{72} + \frac{93267t_c^4}{1280} - \frac{60971t_c^5}{160} \\ &+ \frac{55988791t_c^6}{26880} - \frac{751063t_c^7}{64} + \frac{96895065201t_c^8}{1433600} + \mathcal{O}(t_c^9), \end{aligned} \tag{4.96}$$

$$\begin{aligned} F_{\text{NS}}^{(2)}(t_c) = &-\frac{7}{2880t_c^2} - \frac{15443t_c}{2880} + \frac{1693691t_c^2}{25600} - \frac{260975t_c^3}{384} + \frac{64632739t_c^4}{10240} \\ &- \frac{703614501t_c^5}{12800} + \frac{937885538851t_c^6}{2048000} \end{aligned} \tag{4.97}$$

The main claim of [17] is that the derivative of the regular part of the quantum free energy is related to the non-perturbative A function of the corresponding quantum mechanical model. For the triangular lattice, we find that

$$\boxed{\begin{aligned} \mathcal{A}_{\text{top}}^{\text{tri}}(B,\phi) &= \sum_n \left(\frac{\phi}{6\sqrt{3}}\right)^{2n-2} \frac{\partial}{\partial B} F_n^{(r)}\left(t_c = -\frac{B\phi}{6\sqrt{3}}\right) = \left[\frac{1}{\hbar}\frac{\partial \mathcal{F}^{(r)}(t_c;\hbar)}{\partial t_c}\right]\Big|_{\substack{\hbar=-\frac{\phi}{6\sqrt{3}} \\ t_c=-\frac{B\phi}{6\sqrt{3}}}}, \\ \mathcal{A}_{\text{btm}}^{\text{tri}}(B,\phi) &= \frac{1}{2}\sum_n \left(\frac{\phi}{3\sqrt{3}}\right)^{2n-2} \frac{\partial}{\partial B} F_n^{(r)}\left(t_c = -\frac{B\phi}{3\sqrt{3}}\right) = \left[\frac{1}{2\hbar}\frac{\partial \mathcal{F}^{(r)}(t_c;\hbar)}{\partial t_c}\right]\Big|_{\substack{\hbar=-\frac{\phi}{3\sqrt{3}} \\ t_c=-\frac{B\phi}{3\sqrt{3}}}}, \end{aligned}} \tag{4.98}$$

where $B := n + 1/2$ and $F_n^{(r)} := F_{\text{NS}}^{(n)r}$ denotes the regular part of the n-th level NS free energy. The singular part of the quantum B-period turns out to be related to the prefactor in (3.54) and

(3.55). We have

$$\begin{aligned}
&\left[\frac{1}{\hbar}\left(\frac{\partial\mathcal{F}_t^{(s)}(t_c;\hbar)}{\partial t_c}-t_c\log\left(-\frac{t_c}{2}\right)\right)\right]\Big|_{\substack{\hbar=-\frac{\phi}{6\sqrt{3}}\\ t_c=-\frac{B\phi}{6\sqrt{3}}}}\\
=&\left[\frac{1}{2\hbar}\left(\frac{\partial\mathcal{F}_b^{(s)}(t_c;\hbar)}{\partial t_c}-2t_c\log(-t_c)\right)\right]\Big|_{\substack{\hbar=-\frac{\phi}{3\sqrt{3}}\\ t_c=-\frac{B\phi}{3\sqrt{3}}}}\\
=&-B-\frac{1}{24B}+\frac{7}{2880B^3}-\frac{31}{40320B^5}+\frac{127}{215040B^7}+\mathcal{O}(B^{-9})\\
=&-B+\sum_{n\geq 1}\frac{(2^{1-2n}-1)B^{1-2n}B_{2n}}{2n(2n-1)}\\
=&\log\Gamma\left(B+\frac{1}{2}\right)-B\log B-\frac{\log 2\pi}{2}
\end{aligned}\tag{4.99}$$

Putting the singular part and the regular part together, we can rewrite the bandwidths of triangular lattice in the form

$$\begin{aligned}
\Delta E_{\text{top}}^{\text{tri}}&=\frac{9}{2\pi}\frac{\partial E_{\text{top}}^{\text{tri pert}}}{\partial n}\exp\left[-\frac{\hat{A}}{\phi}-\frac{1}{\hbar}\left(\frac{\partial\mathcal{F}_t(t_c;\hbar)}{\partial t_c}\right)\right]+\cdots,\\
\Delta E_{\text{btm}}^{\text{tri}}&=\frac{3}{2\pi}\frac{\partial E_{\text{btm}}^{\text{tri pert}}}{\partial n}\exp\left[-\frac{\hat{A}}{5\phi}-\frac{1}{2\hbar}\left(\frac{\partial\mathcal{F}_b(t_c;\hbar)}{\partial t_c}\right)\right]+\cdots,
\end{aligned}\tag{4.100}$$

where we have abbreviated the identifications for convenience.

If we do some modification of the instanton action and the free energy, we can get the correspondence between quantum free energy of local $\mathcal{B}_3$ and the A-function of redefined energy λ of the honeycomb lattice, as first shown in [21]. The modified instanton action near the top and bottom edge is given by

$$A^{\text{top}}(\hbar):=\frac{2}{i}\int_{-\pi/2}^{\pi/2}dx\arccos\left(\frac{3\cos(\hbar/6)}{2\cos x}-\frac{\cos(2x-\hbar/2)}{2\cos x}\right),\tag{4.101}$$

$$A^{\text{btm}}(\hbar):=-\frac{1}{i}\text{Im}\int_{-\pi/2}^{\pi/2}dx\arccos\left(\frac{3-6\cos(\hbar/3)}{8\sin\left(\frac{\pi}{6}-\frac{\hbar}{6}\right)\cos x}-\frac{\cos(2x-\hbar/2)}{2\cos(x)}\right).\tag{4.102}$$

Since we don't know explicitly how the free energy transforms from the Weyl quantization method (4.4) to the second quantization method (4.69) , We will set the mass parameters to $m_1=m_2=$

$m_3 = q^{-1/6}$ and use the Weyl quantization, which is equivalent to the second quantization method with $m_i = 1$. Since the mass parameters depend on the quantization deformation parameter, the conifold points that corresponds to $\lambda = 6$ and $\lambda = -3$ gets modified to

$$z = \frac{1}{6\cos\frac{\hbar}{6}}, \qquad z = \frac{2\sin\left(\frac{\pi}{6} - \frac{\hbar}{6}\right)}{3 - 6\cos\frac{\hbar}{6}}. \tag{4.103}$$

Using the method in Appendix A, one can calculate the NS free energy taking values at $m_i = q^{-1/6}$, the quantum B-period is indeed related to the non-perturbative A function of the honeycomb lattice, as shown in [21]. We summarize the results [2] as follows:

$$\boxed{\begin{aligned}\mathcal{A}^{\text{honeycomb}}_{\text{top}}(n,\phi) &= \left[-\frac{A^{\text{top}}(\hbar)}{\hbar} + \frac{\sqrt{3}}{\hbar}\left(\frac{\partial\mathcal{F}^{(r)}(t_c,\hbar)}{\partial t_c}\right)\right]\Big|_{\substack{\hbar=-\phi \\ t_c=-\frac{B\phi}{\sqrt{3}}}}, \\ \mathcal{A}^{\text{honeycomb}}_{\text{btm}}(n,\phi) &= \left[-\frac{A^{\text{btm}}(\hbar)}{\hbar} + \frac{\sqrt{3}}{\hbar}\left(\frac{\partial\mathcal{F}^{(r)}(t_c;\hbar)}{\partial t_c}\right)\right]\Big|_{\substack{\hbar=-\phi \\ t_c=-\frac{B\phi}{3\sqrt{3}}}},\end{aligned}} \tag{4.104}$$

where we have absorbed $\hat{A}/\phi$ into the instanton fluctuation. The singular part of the quantum B-period near the top edge is identical to its counterpart of the triangular lattice. For the bottom edge, we have

$$\left[\frac{\sqrt{3}}{\hbar}\left(\frac{\partial\mathcal{F}^{(s)}(t_c;\hbar)}{\partial t_c}\right)\right]\Big|_{\substack{\hbar=-\phi \\ t_c=-\frac{B\phi}{3\sqrt{3}}}} = n\log\left(\frac{\phi}{3\sqrt{3}}\right) + \log\Gamma(n) + \frac{1}{2}\log n - \frac{\log 2\pi}{2}. \tag{4.105}$$

Then the bandwidths near the top and bottom edge for honeycomb lattice can be rewritten as

$$\begin{aligned}\Delta\lambda_{\text{top}} &= \frac{9}{2\pi}\frac{\partial\lambda^{\text{pert}}_{\text{top}}}{\partial n}\exp\left[\frac{A^{\text{top}}(\hbar)}{\hbar} - \frac{\sqrt{3}}{\hbar}\left(\frac{\partial\mathcal{F}_t(t_c;\hbar)}{\partial t_c}\right)\right] + \cdots, \\ \Delta\lambda_{\text{btm}} &= 3^{3/4}\frac{\partial\lambda^{\text{pert}}_{\text{btm}}}{\partial n}\exp\left[\frac{A^{\text{btm}}(\hbar)}{\hbar} - \frac{\sqrt{3}}{\hbar}\left(\frac{\partial\mathcal{F}_b(t_c;\hbar)}{\partial t_c}\right)\right] + \cdots.\end{aligned} \tag{4.106}$$

Finally we would like to calculate the free energy of local $\mathbb{F}_0$ near the conifold point. The

[2] Here the scaling of t_c in the free energy differs from the one for the triangular lattice. And there's no t_c term in the exponential on the right hand side as in [21]. This term can be removed by shifting τ by a constant.

modulus of the conifold frame is related to the large radius frame by $z_c = 1/16 - z$. The flat coordinate and the prepotential are given as the solutions of the Picard-Fuchs equations for local $\mathbb{F}_0$ with the conifold coordinate. The series solutions are given by

$$\begin{aligned} t_c =& z_c + 10z_c^2 + \frac{356z_c^3}{3} + 1524z_c^4 + \frac{102436z_c^5}{5} + \frac{851240z_c^6}{3} \\ &+ \frac{28093456z_c^7}{7} + 57659240z_c^8 + \mathcal{O}(z_c^9), \end{aligned} \tag{4.107}$$

$$\begin{aligned} t_D = \frac{\partial F_0}{\partial t_c} =& t_c \log z_c + t_c + 9z_c^2 + \frac{1348z_c^3}{9} + \frac{6713z_c^4}{3} + \frac{2466662z_c^5}{75} \\ &+ \frac{21769952z_c^6}{45} + \frac{1051128088z_c^7}{147} + \mathcal{O}(z_c^8). \end{aligned} \tag{4.108}$$

From these relations, we can get the prepotential

$$F_0(t_c) = t_c^2\left(\frac{\log -t_c}{2} - \frac{3}{4}\right) - \frac{t_c^3}{3} + \frac{5t_c^4}{18} - \frac{7t_c^5}{15} + \frac{733t_c^6}{675} - \frac{188t_c^7}{63} + \frac{35921t_c^8}{3969} + \mathcal{O}(t_c^9). \tag{4.109}$$

The first correction of the NS free energy is

$$F_{\text{NS}}^{(1)} = \frac{1}{24}\log\left[\frac{1}{z_c}(\frac{1}{16} - z_c)^2\right], \tag{4.110}$$

whose expansion in terms of the mirror map is given by

$$\begin{aligned} F_{\text{NS}}^{(1)} =& -\frac{1}{24}\log t_c - \frac{11t_c}{12} + \frac{49t_c^2}{36} - \frac{77t_c^3}{18} + \frac{2213t_c^4}{135} - \frac{607t_c^5}{9} \\ &+ \frac{2443337t_c^6}{8505} - \frac{1183937t_c^7}{945} + \mathcal{O}(t_c^8). \end{aligned} \tag{4.111}$$

Using the tools in Appendix A, we can also write the next few corrections of NS free energy in compact form. For instance, the second level is given by

$$F_{\text{NS}}^{(2)} = -\frac{(k_2+k_3)^2}{54k_2^2k_3}E_2(\tau) - \frac{775k_2^3 + 1031k_2^2k_4 + 2112k_2k_4^2 + 1264k_4^3}{4320k_2^2k_3}, \tag{4.112}$$

where we have taken the holomorphic limit and

$$k_i := \vartheta_i^4(q), \qquad q := e^{i\pi\tau}. \tag{4.113}$$

Expanding in terms of the mirror map, we get

$$\begin{aligned} F_{\text{NS}}^{(2)} = &-\frac{7}{5760t_c^2} - \frac{889t_c}{720} + \frac{181981t_c^2}{10800} - \frac{16157t_c^3}{108} + \frac{2194733t_c^4}{1944} \\ &- \frac{42157069t_c^5}{5400} + \frac{24840469741t_c^6}{486000} - \frac{261024263t_c^7}{810} + \mathcal{O}(t_c^8). \end{aligned} \tag{4.114}$$

It was proposed in [20] that the non-perturbative A function for the square lattice is related to the regular part of the quantum B-period. The result is given as follows

$$\boxed{\mathcal{A}^{\text{square}}(n,\phi) = \sum_n \left(\frac{\phi}{16}\right)^{2n-2} \frac{\partial}{\partial B} F_n^{(r)}\left(t_c = -\frac{B\phi}{16}\right) = \left[\frac{1}{\hbar}\left(\frac{\partial \mathcal{F}^{(r)}(t_c;\hbar)}{\partial t_c}\right)\right]\Bigg|_{\substack{\hbar=-\phi/16 \\ t_c=-\frac{B\phi}{16}}}}. \tag{4.115}$$

The derivative of the singular part of the quantum free energy gives the prefactor in (3.46)

$$\left[\frac{1}{\hbar}\left(\frac{\partial \mathcal{F}^{(s)}(t_c;\hbar)}{\partial t_c}\right)\right]\Bigg|_{\substack{\hbar=-\phi/16 \\ t_c=-\frac{B\phi}{16}}} = \log\left(\frac{\Gamma(B+\frac{1}{2})}{\sqrt{2\pi}}\left(\frac{\phi}{16}\right)^B\right). \tag{4.116}$$

Therefore the bandwidths of the square lattice can be rewritten in the form

$$\Delta E^{\text{square}} = \frac{4}{\pi}\frac{\partial E^{\text{square pert}}}{\partial n} \exp\left[-\frac{A}{\phi} - \frac{1}{\hbar}\left(\frac{\partial \mathcal{F}(t_c;\hbar)}{\partial t_c}\right)\right] + \cdots. \tag{4.117}$$

with the identifications $\hbar = -\phi/16, t_c = -B\phi/16$.

4.3 The Dictionary

From the investigations above, it's clear that the quantization of local $\mathcal{B}_3$ geometry with appropriate choice of mass parameters and quantization method corresponds to Harper-Hofstadter model on square lattice, triangular lattice and honeycomb lattice. We summarize the topological string/ condensed matter correspondence in the following tables 4.2, 4.3 and 4.4.

Table 4.2: The dictionary of the TS/CM correspondence

Topological String on local CY manifold	Condensed Matter Physics
Weyl quantization of the mirror curve of local $\mathcal{B}_3$	Hamiltonian H_{tri}
Quantization of the mirror curve of local $\mathcal{B}_3$ by promoting $e^{ax+by} \to e^{a\hat{x}}e^{b\hat{y}}$	Hamiltonian $H_{\text{honeycomb}}$
Quantum curve of local $\mathbb{F}_0$	Hamiltonian H_{square}
Planck constant $\hbar$	magnetic flux ϕ
Mass parameters $\mathbf{m}$	Hopping parameters λ
Branch cut structure of $t(\mathcal{E};\hbar)$	Hofstadter's butterfly
Imaginary part of $\frac{\partial t}{\partial \mathcal{E}}$	Density of States
$t(\mathcal{E};\hbar)$ evaluated at the conifold point	Instanton action
Quantum B-period	Non-perturbative A function

Table 4.3: The TS/CM correspondence for local $\mathcal{B}_3$ with isotropic mass parameters

Topological String on local $\mathcal{B}_3$	Condensed Matter Physics	
	Weyl quantization	Quantization: $e^{ax+by} \to e^{a\hat{x}}e^{b\hat{y}}$
Conifold point $\mathcal{E} = 6$	top edge of the band spectrum for the triangular lattice	top edge of the band spectrum for the honeycomb lattice
Conifold point $\mathcal{E} = -3$	bottom edge of the band spectrum for the triangular lattice	bottom edge of the band spectrum for the honeycomb lattice
Conifold point $\mathcal{E} = -2$	van Hove singularity at $\phi = 0$	

Table 4.4: The TS/CM correspondence for local $\mathbb{F}_0$ with isotropic mass parameters

Topological String on local $\mathbb{F}_0$	Condensed Matter Physics
Conifold point $z = \frac{1}{16}$	top and bottom edge of the band spectrum for the square lattice
Orbifold point $z = \infty$	van Hove singularity at $\phi = 0$

One useful application of this dictionary would be calculation of the quantum free energy. If one can compute the non-perturbative A function from the condensed matter side to relatively high orders, then we can simply integrate to get the quantum free energy with appropriate identifications of parameters.

5. SUMMARY AND DISCUSSIONS

In this dissertation, we have demonstrated the correspondence between topological string theory on some local CY manifolds and the Harper-Hofstadter model on certain lattices. The main structure of the correspondence is summarized in 5.1. Specifically, we have shown that the quantum A-period $t(\mathcal{E};\hbar)$ can be written in closed form using the secular equation coming from the condensed matter side. Conversely, the DOS equals the derivative of $t(\mathcal{E};\hbar)$. The Hofstadter's butterfly turns out to be identical to the branch cut structure of $t(\mathcal{E};\hbar)$. In order to extract the information of the non-perturbative A function, which is conjectured to be equal to the quantum B-period, we analyzed the bandwidths near the edges of the spectrum in great detail. It's shown that the quantum B-period indeed equals the corresponding non-perturbative A function with an appropriate identification of parameters.

There are some open problems worth pursuing in the future. In this thesis we mainly focus on the perturbative sector, one-instanton sector and the instanton-anti-instanton sector for the semi-classical analysis. It would be interesting to calculate the higher instanton corrections and see whether it corresponds to any quantity in the topological string side. Numerically speaking, it would be a quite challenging task since for the flux of order $\sim \mathcal{O}(10^{-2})$, the two-instanton correction would be of order $\sim \mathcal{O}(e^{-100A})$, the computational power required would be more and more costly as we investigate higher and higher instanton corrections. Another interesting question to

Table 5.1: The TS/CM correspondence

Topological String Side		Condensed Matter Theory Side
Local $\mathcal{B}_3$	$\longrightarrow$	Triangular Lattice
$\downarrow$	$\searrow$	
		Honeycomb Lattice
Local $\mathbb{F}_0$	$\longrightarrow$	Square Lattice

consider regards the ambiguity of quantizing the term e^{ax+by}. The choice of quantization method is easily reflected in the calculation of quantum A-period. However, computation of the quantum free energy using the holomorphic anomaly equations seems to favour the Weyl quantization only. It's natural to ask how the quantum free energy transforms as we shift from one quantization method to another.

REFERENCES

[1] E. Witten, "Topological quantum field theory," *Communications in Mathematical Physics*, vol. 117, no. 3, pp. 353–386, 1988.

[2] N. Drukker, M. Marino, and P. Putrov, "From weak to strong coupling in abjm theory," *Communications in mathematical physics*, vol. 306, no. 2, pp. 511–563, 2011.

[3] N. Drukker, M. Marino, and P. Putrov, "Nonperturbative aspects of ABJM theory," *Journal of High Energy Physics*, vol. 2011, no. 11, pp. 1–29, 2011.

[4] M. Marino and P. Putrov, "Abjm theory as a fermi gas," *Journal of Statistical Mechanics: Theory and Experiment*, vol. 2012, no. 03, p. P03001, 2012.

[5] Y. Hatsuda, S. Moriyama, and K. Okuyama, "Exact Results on the ABJM Fermi Gas," *JHEP*, vol. 10, p. 020, 2012.

[6] A. Grassi, Y. Hatsuda, and M. Marino, "Topological Strings from Quantum Mechanics," *Annales Henri Poincare*, vol. 17, no. 11, pp. 3177–3235, 2016.

[7] J. Gu, A. Klemm, M. Marino, and J. Reuter, "Exact solutions to quantum spectral curves by topological string theory," *Journal of High Energy Physics*, vol. 2015, no. 10, pp. 1–69, 2015.

[8] S. Codesido, J. Gu, and M. Marino, "Operators and higher genus mirror curves," *JHEP*, vol. 02, p. 092, 2017.

[9] Y. Hatsuda and M. Marino, "Exact quantization conditions for the relativistic toda lattice," *Journal of High Energy Physics*, vol. 2016, no. 5, pp. 1–35, 2016.

[10] X. Wang, G. Zhang, and M.-x. Huang, "New Exact Quantization Condition for Toric Calabi-Yau Geometries," *Phys. Rev. Lett.*, vol. 115, p. 121601, 2015.

[11] N. A. Nekrasov and S. L. Shatashvili, "Quantization of Integrable Systems and Four Dimensional Gauge Theories," in *Proceedings, 16th International Congress on Mathematical Physics (ICMP09): Prague, Czech Republic, August 3-8, 2009*, pp. 265–289, 2009.

[12] K. Sun, X. Wang, and M.-x. Huang, "Exact quantization conditions, toric calabi-yau and non-perturbative topological string," *Journal of High Energy Physics*, vol. 2017, no. 1, pp. 1–102, 2017.

[13] Y. Hatsuda, H. Katsura, and Y. Tachikawa, "Hofstadter's butterfly in quantum geometry," *New Journal of Physics*, vol. 18, no. 10, p. 103023, 2016.

[14] D. R. Hofstadter, "Energy levels and wave functions of bloch electrons in rational and irrational magnetic fields," *Phys. Rev. B*, vol. 14, pp. 2239–2249, Sep 1976.

[15] Y. Hatsuda, Y. Sugimoto, and Z. Xu, "Calabi-yau geometry and electrons on 2d lattices," *Physical Review D*, vol. 95, no. 8, p. 086004, 2017.

[16] F. H. Claro and G. H. Wannier, "Magnetic subband structure of electrons in hexagonal lattices," *Phys. Rev. B*, vol. 19, pp. 6068–6074, Jun 1979.

[17] S. Codesido and M. Marino, "Holomorphic anomaly and quantum mechanics," *Journal of Physics A: Mathematical and Theoretical*, vol. 51, no. 5, p. 055402, 2017.

[18] J. Zinn-Justin and U. D. Jentschura, "Multi-instantons and exact results i: Conjectures, wkb expansions, and instanton interactions," *Annals of Physics*, vol. 313, no. 1, pp. 197–267, 2004.

[19] J. Zinn-Justin and U. D. Jentschura, "Multi-instantons and exact results ii: Specific cases, higher-order effects, and numerical calculations," *Annals of Physics*, vol. 313, no. 2, pp. 269–325, 2004.

[20] Z. Duan, J. Gu, Y. Hatsuda, and T. Sulejmanpasic, "Instantons in the hofstadter butterfly: difference equation, resurgence and quantum mirror curves," *Journal of High Energy Physics*, vol. 2019, no. 1, pp. 1–45, 2019.

[21] Y. Hatsuda and Y. Sugimoto, "Bloch electrons on honeycomb lattice and toric calabi-yau geometry," *Journal of High Energy Physics*, vol. 2020, no. 5, pp. 1–19, 2020.

[22] R. Rammal, "Landau level spectrum of bloch electrons in a honeycomb lattice," *Journal de Physique*, vol. 46, no. 8, pp. 1345–1354, 1985.

[23] R. Gopakumar and C. Vafa, "M theory and topological strings. 2.," 1998.

[24] M.-x. Huang and A. Klemm, "Direct integration for general Ω backgrounds," *Adv. Theor. Math. Phys.*, vol. 16, no. 3, pp. 805–849, 2012.

[25] D. Krefl and J. Walcher, "Extended Holomorphic Anomaly in Gauge Theory," *Lett. Math. Phys.*, vol. 95, pp. 67–88, 2011.

[26] A. Iqbal, C. Kozcaz, and C. Vafa, "The refined topological vertex," *Journal of High Energy Physics*, vol. 2009, no. 10, p. 069, 2009.

[27] T. M. Chiang, A. Klemm, S.-T. Yau, and E. Zaslow, "Local mirror symmetry: Calculations and interpretations," *Adv. Theor. Math. Phys.*, vol. 3, pp. 495–565, 1999.

[28] M. Aganagic, A. Klemm, and C. Vafa, "Disk instantons, mirror symmetry and the duality web," *Z. Naturforsch.*, vol. A57, pp. 1–28, 2002.

[29] O. Aharony, O. Bergman, D. L. Jafferis, and J. Maldacena, "N=6 superconformal Chern-Simons-matter theories, M2-branes and their gravity duals," *JHEP*, vol. 10, p. 091, 2008.

[30] Y. Hatsuda, M. Marino, S. Moriyama, and K. Okuyama, "Non-perturbative effects and the refined topological string," *JHEP*, vol. 09, p. 168, 2014.

[31] Y. Hatsuda, "Comments on exact quantization conditions and non-perturbative topological strings," *arXiv preprint arXiv:1507.04799*, 2015.

[32] G. Lockhart and C. Vafa, "Superconformal partition functions and non-perturbative topological strings," *Journal of High Energy Physics*, vol. 2018, no. 10, pp. 1–43, 2018.

[33] Y. Hasegawa, Y. Hatsugai, M. Kohmoto, and G. Montambaux, "Stabilization of flux states on two-dimensional lattices," *Physical review B*, vol. 41, no. 13, p. 9174, 1990.

[34] Y. Hatsugai and M. Kohmoto, "Energy spectrum and the quantum hall effect on the square lattice with next-nearest-neighbor hopping," *Physical review B*, vol. 42, no. 13, p. 8282, 1990.

[35] C. M. Bender and T. T. Wu, "Anharmonic oscillator," *Physical Review*, vol. 184, no. 5, p. 1231, 1969.

[36] C. M. Bender and T. T. Wu, "Anharmonic oscillator. ii. a study of perturbation theory in large order," *Physical Review D*, vol. 7, no. 6, p. 1620, 1973.

[37] T. Sulejmanpasic and M. Ünsal, "Aspects of perturbation theory in quantum mechanics: The benderwu mathematica® package," *Computer Physics Communications*, vol. 228, pp. 273–289, 2018.

[38] I. Aniceto, G. Başar, and R. Schiappa, "A primer on resurgent transseries and their asymptotics," *Physics Reports*, vol. 809, pp. 1–135, 2019.

[39] Y. Hatsuda, "Perturbative/nonperturbative aspects of bloch electrons in a honeycomb lattice," *Progress of Theoretical and Experimental Physics*, vol. 2018, no. 9, p. 093A01, 2018.

[40] K. Esaki, M. Sato, M. Kohmoto, and B. I. Halperin, "Zero modes, energy gap, and edge states of anisotropic honeycomb lattice in a magnetic field," *Physical Review B*, vol. 80, no. 12, p. 125405, 2009.

[41] M. Ezawa, "Supersymmetry and unconventional quantum hall effect in graphene," *arXiv preprint cond-mat/0606084*, 2006.

[42] G. V. Dunne and M. Unsal, "What is qft? resurgent trans-series, lefschetz thimbles, and new exact saddles," *arXiv preprint arXiv:1511.05977*, 2015.

[43] O. Aharony, A. Hanany, and B. Kol, "Webs of (p, q) 5-branes, five dimensional field theories and grid diagrams," *Journal of High Energy Physics*, vol. 1998, no. 01, p. 002, 1998.

[44] N. Seiberg, "Five dimensional susy field theories, non-trivial fixed points and string dynamics," *Physics Letters B*, vol. 388, no. 4, pp. 753–760, 1996.

[45] M.-x. Huang, A. Klemm, and M. Poretschkin, "Refined stable pair invariants for e-, m-and [p, q]-strings," *Journal of High Energy Physics*, vol. 2013, no. 11, pp. 1–118, 2013.

[46] A. Brini and A. Tanzini, "Exact results for topological strings on resolved y p, q singularities," *Communications in Mathematical Physics*, vol. 289, no. 1, pp. 205–252, 2009.

[47] M. Aganagic, A. Klemm, M. Marino, and C. Vafa, "The topological vertex," *Communications in mathematical physics*, vol. 254, no. 2, pp. 425–478, 2005.

[48] M. Aganagic, M. C. Cheng, R. Dijkgraaf, D. Krefl, and C. Vafa, "Quantum geometry of refined topological strings," *Journal of High Energy Physics*, vol. 2012, no. 11, pp. 1–53, 2012.

[49] L. Faddeev, "Modular double of a quantum group," in *Fifty Years of Mathematical Physics: Selected Works of Ludwig Faddeev*, pp. 523–530, World Scientific, 2016.

[50] M. Bershadsky, S. Cecotti, H. Ooguri, and C. Vafa, "Holomorphic anomalies in topological field theories," *Nuclear Physics B*, vol. 405, no. 2-3, pp. 279–304, 1993.

[51] M. Bershadsky, S. Cecotti, H. Ooguri, and C. Vafa, "Kodaira-spencer theory of gravity and exact results for quantum string amplitudes," *Communications in Mathematical Physics*, vol. 165, no. 2, pp. 311–427, 1994.

[52] T. W. Grimm, A. Klemm, M. Marino, and M. Weiss, "Direct integration of the topological string," *Journal of High Energy Physics*, vol. 2007, no. 08, p. 058, 2007.

[53] A. Hanany and E. Witten, "Type IIB superstrings, BPS monopoles, and three-dimensional gauge dynamics," *Nuclear Physics B*, vol. 492, no. 1-2, pp. 152–190, 1997.

APPENDIX A

REFINED HOLOMORPHIC ANOMALY

The refined holomorphic anomaly equations are useful tools to calculate the NS free energy near the conifold point. The general refined holomorphic anomaly equations for local Calabi-Yau manifold read

$$\frac{\partial F^{(g_1,g_2)}}{\partial \bar{t}_k} = \frac{1}{2\gamma}\bar{C}^{lm}_{\bar{k}}\left(D_l D_m F^{(g_1,g_2-1)} + \sum_{0<r_1+r_2<g_1+g_2} D_l F^{(r_1,r_2)} D_m F^{(g_1-r_1,g_2-r_2)}\right), \tag{A.1}$$

where γ is a constant that depends on the choice of normalization and $\bar{C}^{lm}_{\bar{k}} = G^{l\bar{p}}G^{m\bar{n}}\bar{C}_{\bar{p}\bar{n}\bar{k}}$ is constructed from the complex conjugate of the Yukawa coupling

$$C_{ijk} = \frac{\partial^3 F_0}{\partial t_i \partial t_j \partial t_k}, \tag{A.2}$$

and the metric $G_{i\bar{j}}$ on the moduli space of complex structures. Since we are considering local CY manifolds, the geometric structure is essentially a Riemann surface we denote as Σ. The metric is thus given by

$$G_{i\bar{j}} = -i\pi(\tau - \bar{\tau})_{ij}, \tag{A.3}$$

where τ is the period matrix of Σ. If we take $g_1 = 0$ in (A.1), we get the standard holomorphic anomaly equation [50, 51]. The NS limit corresponds to $g_2 = 0$ and in the NS limit (A.1) simplifies to

$$\frac{\partial F^{(n)}_{\text{NS}}}{\partial \bar{t}_k} = \frac{1}{2\gamma}\bar{C}^{lm}_{\bar{k}}\sum_{r=1}^{n-1} D_l F^{(r)}_{\text{NS}} D_m F^{(n-r)}_{\text{NS}}, \qquad n \geq 2, \tag{A.4}$$

where

$$F^{(n)}_{\text{NS}} := F^{(n,0)}. \tag{A.5}$$

If we know $F_{\text{NS}}^{(1)}$ then using (A.4) we can in principle calculate NS free energy to arbitrarily high orders recursively, up to a purely holomorphic dependence on the moduli which is the so called holomorphic ambiguity. It was shown in [25, 24] that

$$F_{\text{NS}}^{(1)} = -\frac{1}{24}\log(\Delta z^a \prod_j m_j^{b_j}), \tag{A.6}$$

where Δ is the discriminant of the curve Σ and the constants a and b_j are determined by requiring regularity at infinity and the information of the geometry we are studying. For genus-1 curves such as local $\mathcal{B}_3$, C_{ijk} only has one component

$$Y = C_{ttt}. \tag{A.7}$$

The propagator, which is an almost holomorphic generator, is defined as

$$\bar{C}_{\bar{t}}^{tt} = \partial_{\bar{t}} S^{tt}. \tag{A.8}$$

The modularity property of $F^{(1)}$ and the relation

$$\partial_t \partial_{\bar{t}} F_{NS}^{(1)} = \frac{1}{2\gamma} C_{ttt} C_{\bar{t}}^{tt}, \tag{A.9}$$

implies that the propagator is proportional to the shifted Eisenstein series:

$$S^{tt} = -\frac{1}{3\beta}\widehat{E_2}(\tau, \bar{\tau}), \tag{A.10}$$

where β is an appropriate constant and $\widehat{E}_2(\tau, \bar{\tau})$ is an almost holomorphic modular form of weight 2 defined by

$$\widehat{E_2}(\tau, \bar{\tau}) = E_2(\tau) - \frac{3}{\pi \tau_2}. \tag{A.11}$$

The elliptic modulus is defined by

$$\tau = \frac{\beta}{2\pi i}\frac{\partial t_D}{\partial t} = \frac{\beta}{2\pi i}\frac{\partial^2 F_0}{\partial t^2}. \tag{A.12}$$

From (A.12), the covariant derivative can be written as

$$D_t = \beta Y D_\tau, \tag{A.13}$$

where D_τ is the Maass derivative acting on modular forms of weight k:

$$D_\tau = \frac{1}{2\pi i}\frac{d}{d\tau} - \frac{k}{4\pi\tau_2}. \tag{A.14}$$

With all these in hand, we can put the holomorphic anomaly equation (A.4) into the form

$$\frac{\partial F_{\text{NS}}^{(n)}}{\partial \widehat{E}_2} = -\frac{\beta}{2\gamma}Y^2 \sum_{r=1}^{n-1} D_\tau F_{\text{NS}}^{(r)} D_\tau F_{\text{NS}}^{(n-r)}, \qquad n \geq 2. \tag{A.15}$$

This can be integrated as

$$F_{\text{NS}}^{(n)} = \sum_{l=1}^{2n-3} c_l^{(n)}(\tau)\widehat{E}_2^l(\tau,\bar{\tau}) + f_n(\tau), \tag{A.16}$$

as shown in [52]. Since $F^{(n)}(\tau,\bar{\tau})$ are non-holomorphic modular forms of weight zero under the appropriate monodromy transformation of Σ, therefore $c_l^{(n)}(\tau)$ are modular forms of weight $-2l$ which can be completely fixed by holomorphic anomaly equations. The holomorphic ambiguity $f_n(\tau)$ can be fixed by a Schwinger loop type computation called the gap condition.

APPENDIX B

HANANY-WITTEN TRANSITIONS FROM LOCAL $\mathcal{B}_3$ TO MASS DEFORMED E_8 DEL PEZZO GEOMETRY

It was shown in [15] that the mirror curve of local $\mathcal{B}_3$ is related to the mirror curve of mass deformed E_8 del Pezzo geometry by a coordinate transformation, which perfectly explains why the eigenvalues of those two quantum curves match with each other. In this appendix we would like to reconfirm this relation by demonstrating that these two geometries are indeed related by Hanany-Witten transitions [1].

In the context of Type IIB string theory, The 7-branes are codimension-two objects which source the axion-dilation field. They are pointlike as seen from the plane where the 5-brane web lives. The axion-dilaton undergoes a monodromy transformation around each 7-brane, which is equivalent to attaching a branch cut with each 7-brane. The monodromy matrix of how axion-dilaton transforms when crossing the branch cut of the (p, q) 7-brane is given by

$$K_{(p,q)} = 1 + \begin{pmatrix} p \\ q \end{pmatrix} \begin{pmatrix} p & q \end{pmatrix} S, \tag{B.1}$$

where p and q are coprime integers and $S := \begin{pmatrix} 0 & -1 \\ 1 & 0 \end{pmatrix}$. In a generalized (p, q)-brane web containing both 5-branes and 7-branes, a (p, q) 5-brane or 7-brane gets transformed to a (p', q') 5-brane or 7-brane when crossing the branch cut of a (P, Q) 7-brane. The transformation rule is given by

$$\begin{pmatrix} p' \\ q' \end{pmatrix} = K_{(P,Q)} \begin{pmatrix} p \\ q \end{pmatrix}. \tag{B.2}$$

So if we start with the brane-web configuration corresponding to local $\mathcal{B}_3$, and in order to get

[1] We are grateful to Futoshi Yagi for explaining this.

the desired configuration, we can pull a (P, Q) 7-brane from infinity into the loop and let the branch cut of it sweep through some parts of the brane web to let those parts undergo monodromy transformation. Notice that the charge at each junction is always conserved, say

$$\sum_i p_i = \sum_i q_i = 0. \tag{B.3}$$

Therefore new branes would be created during each Hanany-Witten transition to preserve charge conservation. After several steps of these Hanany-Witten transitions [53, 43] together with some global $\mathrm{SL}(2, \mathbb{Z})$ transformations, we finally obtain the web diagram for mass deformed E_8 del Pezzo geometry. We show detailed steps in Fig. B.1.

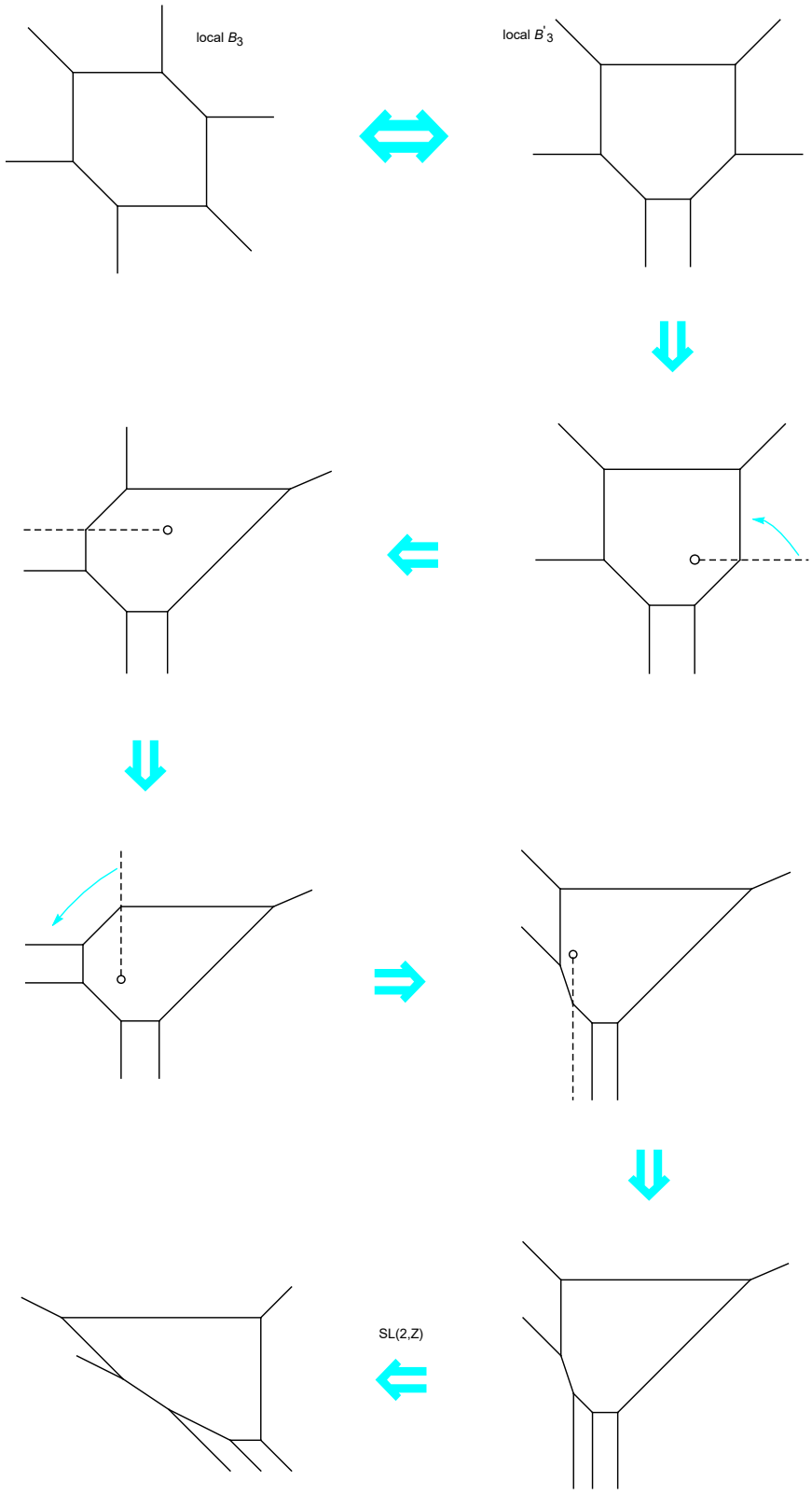

Figure B.1: Hanany-Witten transtions from local $\mathcal{B}_3$ to mass deformed E_8 del Pezzo geometry in detailed steps. The branch cuts are depicted in dashed lines.